JOURNAL OF GEOPHYSICAL RESEARCH, VOL. 111, D22302, doi:10.1029/2005JD006966, 2006

Carbon monoxide: A quantitative tracer for fossil fuel CO_2?

Ulrike Gamnitzer,[1,2] Ute Karstens,[3] Bernd Kromer,[4] Rolf E. M. Neubert,[5] Harro A. J. Meijer,[5] Hartwig Schroeder,[1] and Ingeborg Levin[1]

Received 8 December 2005; revised 9 August 2006; accepted 17 August 2006; published 18 November 2006.

[1] Carbon monoxide (CO), carbon dioxide (CO_2), and radiocarbon ($^{14}CO_2$) measurements have been made in Heidelberg from 2001 to 2004 in order to determine the regional fossil fuel CO_2 component and to investigate the application of CO as a quantitative tracer for fossil fuel CO_2 (CO_2(foss)). The observations were compared with model estimates simulated with the regional transport model REMO at $0.5° \times 0.5°$ resolution in Europe for 2002. These estimates are based on two available emissions inventories for CO and CO_2(foss) and simplified atmospheric chemistry of CO. Both emissions inventories appear to overestimate fossil fuel emissions in the Heidelberg catchment area, in particular in summer and autumn by up to a factor of 2. Nevertheless, during meteorological conditions with high local source influence the CO/CO_2(foss) emission ratios compared well with the observed atmospheric CO/CO_2(foss) ratios. For a larger catchment area of several 100 km the observed CO/CO_2(foss) ratio compared within better than 25% with the ratios derived from model simulations that take the transport from the sites of emission to the measurement station into account. Non-fossil-fuel CO emissions, production by volatile organic compounds, and oxidation, as well as soil uptake, turned out to add significant uncertainty to the application of CO as a quantitative fossil fuel CO_2 surrogate tracer, so that $^{14}CO_2$ measurements seem to be indispensable for reliable estimates of fossil fuel CO_2 over the European continent.

Citation: Gamnitzer, U., U. Karstens, B. Kromer, R. E. M. Neubert, H. A. J. Meijer, H. Schroeder, and I. Levin (2006), Carbon monoxide: A quantitative tracer for fossil fuel CO_2?, *J. Geophys. Res.*, *111*, D22302, doi:10.1029/2005JD006966.

1. Introduction

[2] Fossil fuel CO_2 emissions are a major component of the European carbon budget. About half of the total CO_2 fluxes in winter originate from fossil fuel burning. Therefore only if we are able to accurately separate fossil fuel CO_2 emissions from total CO_2 fluxes on the continental scale will we be able to assess the role of the continental biosphere as a net source or sink of carbon. This will provide a deeper understanding of global carbon cycle dynamics and allow prediction of the future development of CO_2 in the atmosphere. Radiocarbon observations in atmospheric CO_2 have proven to be an excellent tracer for fossil fuel CO_2 in the atmosphere on the regional [*Levin et al.*, 1980, 1989, 2003; *Turnbull et al.*, 2006], the continental [*Tans et al.*, 1979; *de Jong and Mook*, 1982], and also on the global scale [*Suess*, 1955; *Stuiver and Quay*, 1981; *Levin and Hesshaimer*, 2000]. One caveat to use this tracer routinely at CO_2 measurement sites is, however, that continuous long-term high-precision $^{14}CO_2$ observations at a temporal resolution of a few hours or less, although principally possible, are in practice too laborious and expensive. Equally important, the sensitivity of the atmospheric $^{14}CO_2$ level to fossil fuel CO_2 is limited: The highest precision obtained today by conventional counting technique of ±2‰ for single measurements allows one to detect fossil fuel CO_2 with an uncertainty of only slightly less than 1 ppm. This is of the same size as typical summer time fossil fuel CO_2 concentrations at continental mountain sites such as Schauinsland in the Black Forest [*Levin et al.*, 2003].

[3] A number of proxies for fossil fuel CO_2 have thus been suggested and used in the past, including man-made trace substances such as chlorofluorocarbons (CFCs), sulfur hexafluoride (SF_6), acetylene (C_2H_2) and in particular carbon monoxide (CO) [*Bakwin et al.*, 1997; *Potosnak et al.*, 1999; *Rivier et al.*, 2006; *Turnbull et al.*, 2006]. The demands for a good proxy for fossil fuel CO_2 are as follows: (1) Its sources should be related in a unique way to those of fossil fuel CO_2, (2) it should be measured easily and precisely with high temporal resolution, and (3) it should behave conservative in the atmosphere or its sink mechanisms should be well understood and accurately to model. None of the tracers mentioned above fulfils all these demands: While CFCs and SF_6 are chemically stable in the troposphere, their emissions are not directly linked to

[1]Institut für Umweltphysik, University of Heidelberg, Heidelberg, Germany.
[2]Now at Lehrstuhl für Grünlandlehre, Technische Universität München, Freising-Weihenstephan, Germany.
[3]Max Planck Institute for Biogeochemistry, Jena, Germany.
[4]Heidelberger Akademie der Wissenschaften, Heidelberg, Germany.
[5]Centrum voor IsotopenOnderzoek, University of Groningen, Groningen, Netherlands.

0148-0227/06/2005JD006966$09.00

those of fossil fuel CO_2, in particular on the regional scale. On a larger continental or hemispheric scale, they may be better suited. In the case of CO, its sources are very closely linked to those of fossil fuel CO_2: any hydrocarbon oxidation process with CO_2 as an end product is to some extent associated with production of CO. However, stability of CO in the atmosphere is very variable with a tropospheric lifetime ranging between a few weeks up to a year, depending on season. Even more important, the CO/CO_2 ratio of different fossil fuel sources, such as domestic heating or emissions from traffic, can vary by orders of magnitude [*Olivier et al.*, 2005; United Nations Framework Convention on Climate Change (UNFCCC), Greenhouse gases database, 2005, available at http://ghg.unfccc.int] questioning the use of this tracer for quantitative estimates, at least in polluted or semipolluted areas where the source mix can be quite variable.

[4] The aim of this study is, therefore, to investigate the potential, and, in particular, the uncertainties and pitfalls when using CO as a quantitative proxy for fossil fuel CO_2 (CO_2(foss)). By conducting quasi-continuous observations of CO_2 mixing ratio and high-precision $^{14}CO_2$ on so-called integrated samples in Heidelberg we were able to determine the regional fossil fuel CO_2 concentration at this site with a temporal resolution of 1–2 weeks. These measurements were linked to quasi-continuous observations of the CO mixing ratio [*Gamnitzer*, 2003]. In addition, a so-called "event sampler" [*Neubert et al.*, 2004; see also *Zondervan and Meijer*, 1996] was used to collect small volume (4 standard liter) whole air, so-called event samples in glass flasks at a temporal resolution of 1–2 hours over a day, respectively a pollution event. These event samples were analyzed for CO_2 and CO by gas chromatography as well as for $^{14}CO_2$ by accelerator mass spectrometry (AMS). For the integrated as well as for the event samples the regional fossil fuel CO_2 component (ΔCO_2(foss)) was calculated by means of ^{14}C and related to the regional CO offset compared to background mixing ratios (ΔCO) in order to determine the $\Delta CO/\Delta CO_2$(foss) ratios for the different sampling periods (two-weekly/weekly integrals and diurnal events).

[5] We then compared the measured regional fossil fuel CO_2 (calculated by means of ^{14}C), the measured ΔCO as well as the measured $\Delta CO/\Delta CO_2$(foss) ratio with respective model estimates calculated with the Regional Model (REMO) on the basis of two different inventories for fossil fuel CO_2 and CO emissions in Europe. This allows us to determine the uncertainties of estimated fossil fuel CO_2 at a regional polluted sampling site which were derived from the following: (1) Continuous measurements of CO and information on the mean CO/CO_2(foss) ratio of the respective emissions in the catchment area of the measurements, available from inventory data; this ΔCO_2(foss) estimated from ΔCO observations is called $\Delta CO_2(\text{foss})^{\text{eb}}$ (eb: emissions based). (2) REMO model estimates for the measurement site based on CO_2(foss) emissions, and corrected for transport errors of the model by means of measured and modeled ^{222}Rn activity; this radon-corrected modeled ΔCO_2(foss) is called $\Delta CO_2(\text{foss})^{\text{Rn-corr}}$. (3) REMO model estimates corrected for model transport errors and to some extent also for deficiencies in the underlying emissions inventory by means of measured and modeled total ΔCO mixing ratios; this CO-corrected modeled ΔCO_2(foss) is called $\Delta CO_2(\text{foss})^{\text{CO-corr}}$.

[6] Being aware of the problem of potentially observing a very variable source mix at the Heidelberg site, depending on the local area of influence, we nevertheless conducted this study in this polluted region because only here we were able to obtain significant fossil fuel signals of CO_2 and CO also in summer. The application of our methods listed above to estimate fossil fuel CO_2 at sites located further away from direct source influence will probably reduce the uncertainty associated with the heterogeneity of CO/CO_2(foss) emissions ratios considerably.

2. Sampling and Measurement Techniques

2.1. Heidelberg Sampling Station

[7] Observations presented here have been conducted at the Institut für Umweltphysik located on the University campus in the western outskirts of Heidelberg (49.4°N, 8.7°E, 116 m a.s.l.). Heidelberg is a medium size city in the densely populated upper Rhine valley located about 20 km southeast of the industrial area of Mannheim/Ludwigshafen. Because of the prevailing westerly airflow in Europe the larger catchment area of the sampling site is southwestern Germany and eastern France. Local winds are further influenced by the topography of the Rhine valley (north-south) and the Neckar valley (to the east), the regional catchment area is, thus, most probably the Heidelberg city area and the Rhine valley. At the institute's building outside air is collected from the roof at about 30 m above local ground. Air aliquots for gas chromatographic analysis (CO and CO_2), event sampling as well as for integrated sampling and subsequent conventional $^{14}CO_2$ analysis, are taken from a permanently flushed sampling line from the southwest (SW) corner running into the laboratory. Comparison of CO mixing ratios at this intake to observations from a second intake at the southeastern (SE) corner in combination with local wind direction indicated an influence of building exhaust at the SE intake during 3% of the time in 2002, but no distinct influence at the SW intake.

2.2. Quasi-continuous Carbon Dioxide Measurement

[8] An automated gas chromatographic (GC) system (HP5890) with flame ionization detector (FID) is used for quasi-continuous analysis of CO_2 (and CH_4) [*Greschner*, 1995; *Levin et al.*, 1999]. Prior to detection at the FID, which has a linear response curve, CO_2 is reduced to CH_4 using a nickel catalyst. The GC is equipped with a second column and with an electron capture detector (ECD) for N_2O and SF_6 analysis [*Schmidt et al.*, 2001]. An inlet system with two sample loops has been installed to supply each detection line with sampling gas. With that system, also the event flask samples are analyzed. For CO_2 and CH_4 separation we use N_2 as a carrier gas and a 1.8 m HaySep Q column, where CH_4 has a retention time of 1.1 min and CO_2 of 1.9 min. This allows sample injection every 5 min. The routine measurement method takes half an hour and includes two standards and two ambient air injections from the SW intake line. In the case of event or other flask sample analysis, only one ambient air measurement from the SW intake line is done in a half hourly interval. Flask sample analysis is performed only during the day.

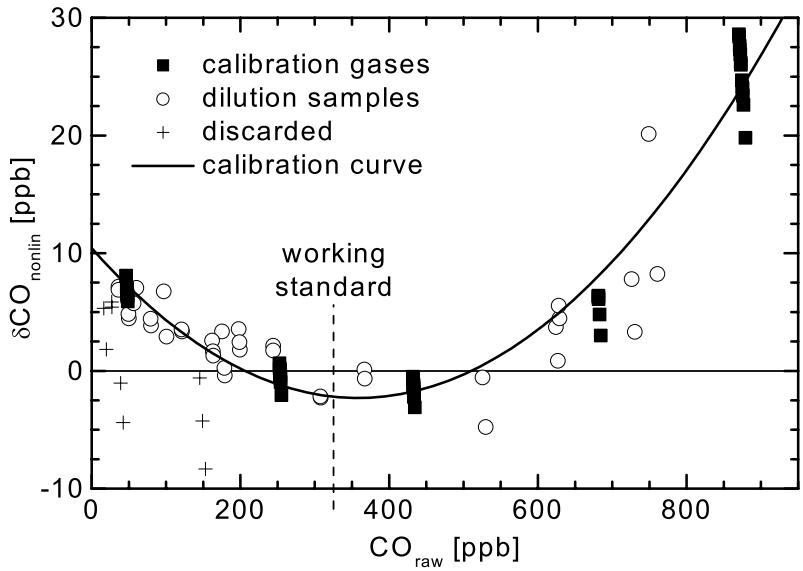

Figure 1. Calibration curve for the Heidelberg CO GC determined with a working standard of 322 ppb. CO_{raw} is the preliminary CO mixing ratio, determined assuming linear response, and $\delta CO_{nonlin} = CO_{true} - CO_{raw}$ is the concentration-dependent correction to be applied to all measurements performed with this working standard.

[9] All CO_2 mixing ratios are reported on the WMO mole fraction scale (X2003) [*Worthy and Huang*, 2005]. The precision of individual analyses is generally better than ±0.1 ppm. As a long-term stability and quality control check we analyze a target gas 4 times every 12 hours. For the period of our study the long-term standard deviation of the half-daily mean target measurements was better than ±0.2 ppm.

2.3. Quasi-continuous Carbon Monoxide Measurement and Calibration

[10] Quasi-continuous analysis of atmospheric CO is carried out with a gas chromatographic system equipped with a mercuric oxide (HgO) reduction gas analyzer (RGA3, Trace Analytics Inc.). For automated measurement an inlet system of valves was installed, which allows flushing of the 1 ml sample loop alternately with a reference gas and different ambient air samples [*Gamnitzer*, 2003]. During the day flask sample analysis is also possible. With synthetic air as a carrier gas the sample is injected onto the GC precolumn (Unibeads 1S, 9.2 m), which is back flushed when H_2 and CO have passed through to the analytical column (Molecular Sieve 5A, 9.2 m; retention time for CO = 1.1 min and for H_2 = 0.5 min). Here H_2 and CO are separated and subsequently carried to a hot HgO bed (265°C), where mercury vapor is produced by oxidation of H_2 and CO. The Hg vapor is detected photometrically via UV absorption.

[11] To quantify CO in an air sample, a working standard with known CO mixing ratio is injected every 15 min, with three samples being analyzed in between. Assuming linear response of the GC system, i.e., that the peak height is proportional to the CO mixing ratio, preliminary mixing ratios (CO_{raw}) are first calculated for each sample. To account for the nonlinearity of the detector response, a correction based on five additional calibration gases is applied to the preliminary mixing ratios.

2.3.1. Calibration of CO Reference Gases

[12] CO mixing ratios are given as mole fractions and are referenced to the volumetric CO scale provided by *Brenninkmeijer et al.* [2001]. All reference gases are dried natural air stored in 40 liter high-pressure aluminium cylinders. The three working standards successively used during the period of this study ranged from 170 ppb to 370 ppb and were calibrated at the Schauinsland station of the German Environmental Agency (Umweltbundesamt). Another five calibration gases ranging from 55 ppb to 900 ppb and handled in the same way as the working standards, were used to determine the nonlinearity correction. At Schauinsland, CO is measured by UV resonance fluorescence spectroscopy since August 2001. This technique shows a linear response [*Gerbig et al.*, 1999] and reference gases with 495 ppb and 1020 ppb CO (±2%), calibrated at the Max Planck Institute for Chemistry (Mainz, Germany), were used there.

2.3.2. Nonlinearity Correction

[13] To assess the nonlinearity of the HgO detector used in Heidelberg for the range of polluted air CO mixing ratios, the five calibration standards were analyzed approximately once per month. In addition 22 samples stored in glass flasks were prepared: Aliquots of the calibration standards were diluted with synthetic air containing 410 ppm CO_2, from which CO and CH_4 had been removed catalytically with platinized quartz wool at 850°C. By means of CH_4 analysis by GC-FID (see section 2.2) in both the calibration standards and the diluted samples the "true" CO mixing ratio (CO_{true}) of the dilution samples was determined.

[14] Between the preliminary and the true mixing ratios of the calibration samples a systematic deviation ($\delta CO_{nonlin} = CO_{true} - CO_{raw}$) was found (see Figure 1 as an example for our working standard at 322 ppb). A quadratic fit was calculated through these deviations, yielding the concentration-

dependent correction, which has to be added to the preliminary mixing ratios determined from the linear response curve to derive calibrated CO mixing ratios. It should be noted that this calibration curve is only used for mixing ratios larger than 70 ppb, i.e., for all measurements presented here. For smaller mixing ratios the calibration curve shows a different shape. A calibration curve has been determined separately for each working standard used. All samples measured against the same working standard were then corrected with one mean calibration curve. The precision of one individual ambient or flask measurement, including the uncertainty of the linearity correction, was estimated to be 0.5–1%.

2.4. Event Sampling

[15] An automated flask sampling system [*Neubert et al.*, 2004] was set up in Heidelberg which enables us to consecutively fill up to twenty 2.5 liter glass containers with outside air: After drying to a dew point of about −40°C the air is flushed through one of the flasks for 1.5 hours at a flow rate of 1.0–1.2 l/min. After flushing, the air sample is pressurized to ∼1 bar overpressure and is stored. The system can be run continuously, filling flask by flask and starting again with the first flask after the last one was filled. The operator can stop sampling at any time and in this way has access to air samples from the last 30 hours. A so-called event is retained when a parallel increase in atmospheric CO_2 and CO mixing ratio (which may occur during low-wind-speed conditions) is observed in the continuous gas chromatographic measurements run simultaneously. Analysis of the event samples with the gas chromatographic systems provided the actual CO_2 and CO mixing ratios in the flasks. The agreement between flask results and continuous measurements was on the order of a few ppm for CO_2 and a few tens ppb for CO. Deviations were random and mainly caused by the large variability in the ambient air signal during events. The relative variability was higher for CO than for CO_2 and thus explains the larger deviations for CO than for CO_2. For further evaluation of the event samples, only the mixing ratios measured on the flask samples were used. After GC analysis CO_2 was extracted from the remaining air via a cold trap (−196°C) at approximately 300 mbar and analyzed for ^{14}C by AMS in the Groningen Radiocarbon Laboratory [*van der Plicht et al.*, 2000]. For individual samples the uncertainty in $\Delta^{14}C$ typically ranged from 5 to 10‰.

2.5. Integrated $^{14}CO_2$ Sampling and Analysis

[16] Integrated atmospheric $^{14}CO_2$ samples have been collected over two weeks in CO_2-free sodium hydroxide solution. Samples were collected only during nighttime (from 1800 to 0600 local time). CO_2 from a total volume of 20–25 m^3 of air was accumulated in one sample for conventional ^{14}C analysis in the Heidelberg Radiocarbon Laboratory. Sampling and analysis techniques are described in detail by *Levin et al.* [1980] and *Kromer and Münnich* [1992]. The $\delta^{13}C$-corrected $\Delta^{14}C$ data are given relative to NBS oxalic acid activity, corrected for decay [*Stuiver and Polach*, 1977]. Internal measurement precision of individual samples is typically $\Delta^{14}C = \pm(2–3)$‰.

2.6. Determination of the Fossil Fuel CO_2 Component

[17] The fossil fuel CO_2 component for event samples or integrated samples was determined from the measured CO_2 mixing ratio and the corresponding $\Delta^{14}CO_2$ according to *Levin et al.* [2003]: The measured CO_2 mixing ratio CO_2(meas) at Heidelberg always consists of three major components, a background component CO_2(bg), a biospheric component CO_2(bio), and a fossil fuel component CO_2(foss) (to avoid confusion with $\Delta^{14}C$ the CO_2 components above background are named CO_2(bio) and CO_2(foss) instead of ΔCO_2(bio) and ΔCO_2(foss)). The $\Delta^{14}C$ of these components are respectively $\Delta^{14}C_{meas}$, $\Delta^{14}C_{bg}$, $\Delta^{14}C_{bio}$ and $\Delta^{14}C_{foss}$. To calculate the fossil fuel CO_2 component, we use the two balance equations for CO_2 mixing ratio and $^{14}C/^{12}C$ ratios (proportional to $(\Delta^{14}C_i + 1000‰)$):

$$CO_2(\text{meas}) = CO_2(\text{bg}) + CO_2(\text{bio}) + CO_2(\text{foss}) \quad (1)$$

$$\begin{aligned} CO_2(\text{meas})\left(\Delta^{14}C_{meas} + 1000‰\right) &= CO_2(\text{bg})\left(\Delta^{14}C_{bg} + 1000‰\right) \\ &+ CO_2(\text{bio})\left(\Delta^{14}C_{bio} + 1000‰\right) \\ &+ CO_2(\text{foss})\left(\Delta^{14}C_{foss} + 1000‰\right). \end{aligned} \quad (2)$$

Assuming that all fossil fuels burned contain no ^{14}C, the fossil fuel term in equation (2) is zero ($\Delta^{14}C_{foss} = -1000‰$). Setting $\Delta^{14}C_{bio}$ equal to $\Delta^{14}C_{bg}$ (about half of the flux from the biosphere comes from autotrophic respiration, a young reservoir in very close ^{14}C equilibrium with atmospheric CO_2, and the remaining heterotrophic respiration flux today is only about 50‰ higher than ambient CO_2 (T. Naegler, personal communication, 2005), and combining both equations then leads to the fossil fuel CO_2 component, further on named ^{14}C-based fossil fuel CO_2 component:

$$CO_2(\text{foss}) = CO_2(\text{meas})\frac{\Delta^{14}C_{bg} - \Delta^{14}C_{meas}}{\Delta^{14}C_{bg} + 1000‰}. \quad (3)$$

For event samples, the background $^{14}CO_2$ values were taken from the measurements of the events themselves: The sample with the lowest CO_2 mixing ratio and the highest $\Delta^{14}CO_2$, normally at the start point of the event, was defined as background. Thus CO_2(foss) represents the portion of fossil fuel CO_2 that has been added to the ambient air during the pile up of the event. For the integrated samples we used the background curves described in section 4.4 and displayed in Figure 8a.

3. Modeling

3.1. Model Description

[18] With the regional online transport model REMO atmospheric CO and CO_2 mixing ratios, as well as ^{222}Rn activities have been simulated. REMO is based on the former operational weather forecast model Europamodell of the German Weather Service [*Majewski*, 1991], and the physical parameterization package of the global climate model ECHAM-4 [*Roeckner et al.*, 1996] is available as an additional option [*Jacob*, 2001]. Modules for tracer transport and tropospheric chemical processes have been implemented to extend REMO to an online atmosphere

chemistry model [*Langmann*, 2000]. REMO has been applied with various trace species modules to investigate the distribution and spatiotemporal variability of ^{222}Rn and CO_2 in Europe and Siberia [*Chevillard et al.*, 2002a, 2002b], to study summer smog episodes in Europe [*Langmann et al.*, 2003] and to simulate the dispersion of particulate matter released by peat fires in Asia [*Langmann and Heil*, 2004].

[19] In the present study REMO (version 5.0), including the ECHAM-4 physical parameterizations, was applied on a semihemispheric domain, which covers the area north of 30°N. The horizontal grid resolution is 0.5° in a rotated spherical coordinate system corresponding to a size of the grid cells of roughly 55 km × 55 km. The model uses the hydrostatic approximation with 20 vertical levels in a hybrid coordinate system with six layers below 1500 m above ground. For the meteorological part analysis data from the European Centre for Medium-Range Weather Forecasts (ECMWF) are used for initialization and as lateral boundary information with a time resolution of six hours. To enable the direct comparison of model results with observations, REMO is run in the so-called forecast mode [e.g., *Karstens et al.*, 1996; *Langmann*, 2000; *Chevillard et al.*, 2002b], in which results of consecutive short-range forecasts (30 hours) for the meteorology are used. To account for a spin-up time, the first six hours of the forecast are neglected. Tracer transport is calculated continuously by simulating only the meteorology in the first six hours of each run, passing the tracer fields directly from the last time step of the previous 30-hour forecast and simulating meteorology and tracer transport during the remaining 24 hours.

[20] The photochemical sources and sinks for CO in the atmosphere are parameterized in REMO on the basis of climatological monthly OH distributions from *Spivakovsky et al.* [2000] and a spatially and temporally constant methane mixing ratio. The strong seasonality of atmospheric OH concentrations, with higher values in summer, produces a pronounced seasonal cycle in the activity of the chemical destruction of atmospheric CO. In order to additionally include the influence of the diurnal OH cycle on atmospheric CO, the seasonal cycle of the climatological OH concentration was folded with a function describing the diurnal cycle of the incoming solar radiation. Soil uptake of CO is parameterized in REMO as dry deposition process, using a constant deposition velocity of 0.03 cm/s [*Sanhueza et al.*, 1998] over vegetated land surfaces.

[21] The CO produced by oxidation of nonmethane volatile organic compounds (VOC) is implemented as a secondary surface source for CO as was done by *Lawrence et al.* [1999], *Shindell et al.* [2001], and *Hauglustaine et al.* [2004]. The spatial distribution of anthropogenic VOC emissions is taken from the Emission Database for Global Atmospheric Research EDGAR 3.2FT2000 [*Olivier et al.*, 2005]. Natural VOC emisssions are based on monthly distributions from *Guenther et al.* [1995], available at the GEIA database (http://www.geiacenter.org). The global amount of these secondary CO emissions from anthropogenic and natural VOCs is then scaled to the total CO emissions given by *Prather et al.* [2001]. Since VOCs have an atmospheric lifetime of at least several hours before they are oxidized the secondary CO emissions are not treated as a pure surface source but distributed vertically in the planetary boundary layer. A diurnal cycle was imposed on the emissions (in the same way as for OH) to restrict the parameterized effect of the VOC oxidation to daytime only.

[22] For a limited area model like REMO, the influences of sources and sinks outside the model domain have to be accounted for by using global mixing ratio fields for the year 2002 as initialization and at the lateral boundaries during the model run. Global CO_2 mixing ratios are provided from the global transport model TM3 [*Heimann and Körner*, 2003] at 6-hour intervals. TM3 was used with a horizontal resolution of 1.9° × 1.9° along with 28 vertical layers. The global distribution of CO is taken from simulations of the global chemistry transport model MOZART [*Horowitz et al.*, 2003] updated every three hours. MOZART (version 2) was used with a horizontal resolution of 1.9° × 1.9° and 31 vertical layers.

3.2. Emissions Inventories

[23] CO and CO_2 emissions from fossil fuel combustion were extracted from two different emissions inventories: (1) The Emission Database for Global Atmospheric Research (EDGAR), which provides annual mean emissions for the base years 1990, 1995 and 2000 on a global 1° × 1° grid [*Olivier et al.*, 2005]. On the basis of international statistics as input data and of emission factors common across countries, it is expected to represent a consistent data set as input for a regional model. (2) At the Institute of Energy Economics and Rational Use of Energy (IER, University of Stuttgart, Germany) a new high-resolution emissions inventory on a 50 km × 50 km grid for the year 2000 and for the greater part of Europe was constructed on the basis of UNFCCC statistics (Y. Scholz and S. Reis, IER, personal communication, 2004). National totals, which were reported to UNFCCC by each country (available at http://ghg.unfccc.int), were disaggregated in time and space, separately for each sector, according to typical diurnal, weekly and seasonal cycles and spatial distributions of point, line and area sources, respectively. A general description of the method is given by *Friedrich et al.* [2003] (available at http://gaia.agraria.unitus.it/ceuroghg/reportws3.pdf). The model used here (IER GENEMIS emission model) was developed as part of GENEMIS (EUROTRAC-2 subproject) [*Friedrich and Reis*, 2004], and the database for temporal and spatial resolution was developed by *Wickert* [2001] (available at http://elib.uni-stuttgart.de/opus/volltexte/2001/928/). Especially the high temporal resolution of the disaggregated IER data set is a substantial improvement compared to EDGAR because it allows a more realistic simulation of the temporal characteristics in the atmospheric tracer mixing ratios. To cover the entire model domain, the IER emissions inventories were complemented by the EDGAR emissions inventories where IER data were missing.

[24] A comparison of annual mean fossil fuel CO and CO_2 emissions and resulting emission ratios in Europe shows regionally large differences between the EDGAR (Figure 2, top) and the IER (Figure 2, bottom) data set because estimates are based on different data sources and also the spatial pattern of emissions and hence emission ratios is strongly dependent on the way national totals are disaggregated. In the REMO simulations for the year 2002 we used the EDGAR and IER emission estimates for 2000

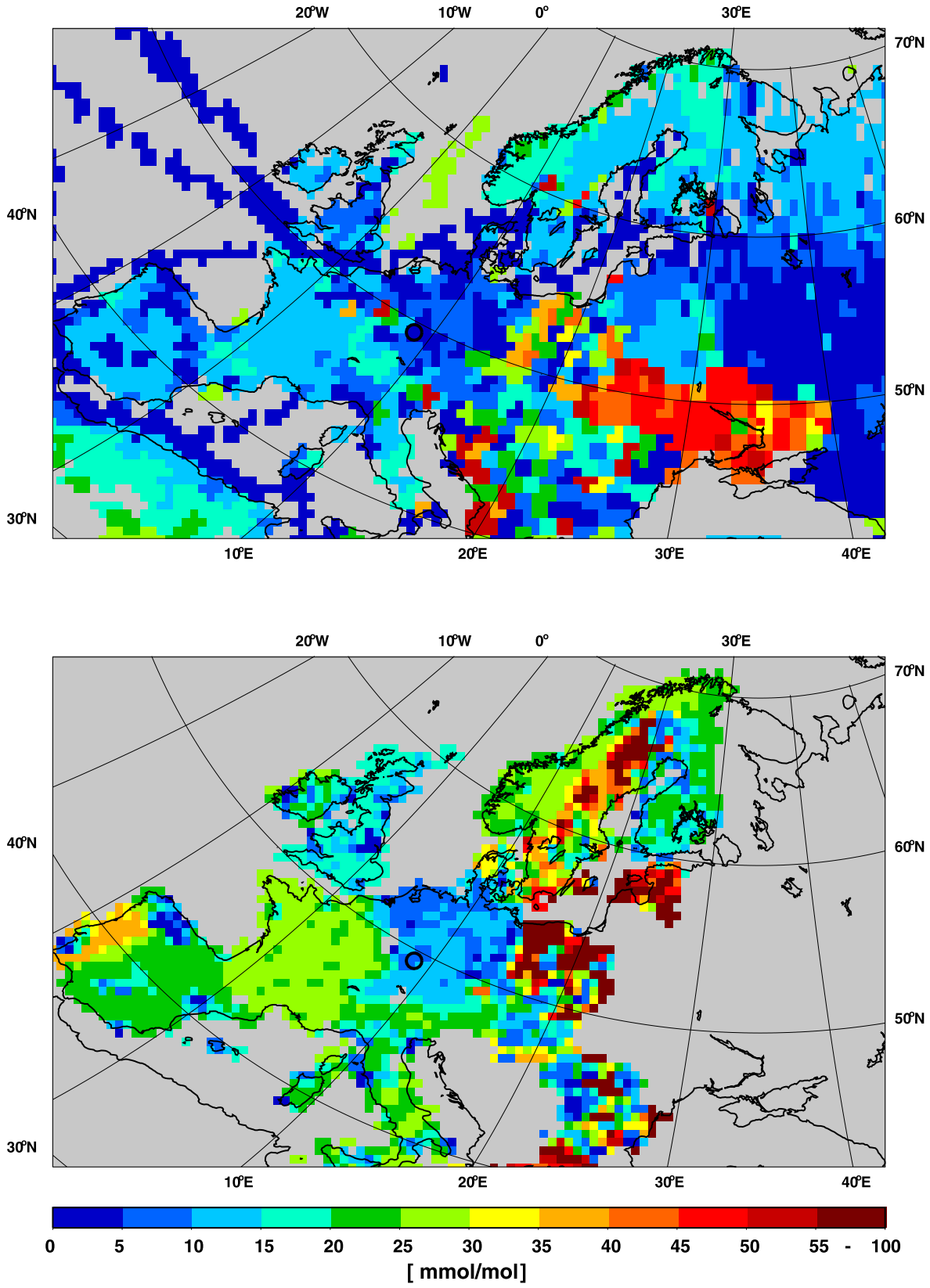

Figure 2. Annual mean CO/CO_2 ratio of fossil fuel emissions only in 2000 from the (top) EDGAR 3.2FT2000 emissions inventory and (bottom) IER emissions inventory. The black circle at about 49°N, 9°E marks the Heidelberg sampling station.

with the latter adjusted for respective weekdays in 2002. Note, however, that the dependency of IER emissions on meteorological parameters such as temperature has not been adjusted to 2002 conditions.

[25] CO surface emissions from sources other than fossil fuel burning were also included in the simulations: Fuel wood burning and agricultural waste burning based on the EDGAR V3.2 inventory [*Olivier et al.*, 2005] with seasonality from *Müller* [1992], biomass burning in the tropics [*Hao and Liu*, 1994] and extra tropics [*Müller*, 1992], biogenic emissions [*Müller*, 1992], and ocean emissions [*Brasseur et al.*, 1998]. When discussing CO/CO_2(foss) ratios from emissions inventories, these non-fossil-fuel surface emissions are added to the fossil fuel CO emissions from EDGAR respectively IER. For the simulation of the total atmospheric CO_2 mixing ratio also biospheric and oceanic CO_2 fluxes need to be included. The biosphere-atmosphere exchange of CO_2 through photosynthesis and respiration is described by the terrestrial biosphere model BIOME-BGC [*Churkina et al.*, 2003] driven by meteorological analyses for 2002 and including a diurnal cycle based on incoming radiation. Ocean fluxes are prescribed according to *Takahashi et al.* [1999].

4. Results and Discussion

4.1. Continuous CO_2 and CO Mixing Ratios

[26] Hourly mean values of quasi-continuously observed CO_2 and CO mixing ratios in Heidelberg are presented in Figures 3 and 4 for January and August 2002 together with respective ^{222}Rn and wind speed observations. The first half of January 2002 was characterized by a number of strong winter inversion situations each lasting for about four to six days. During these typical anticyclonic weather situations over Western Europe temperatures were very low with calm winds from the North and little atmospheric mixing. All atmospheric trace gases with sources on or close to the ground, and in particular CO_2 and CO increased to very high levels, in the first episode CO_2 up to 550 ppm and CO up to 2000 ppb. The general shape of the increase is very similar for CO_2 and CO. Whole air event samples were collected at the beginning of this first episode on 4 and 5 January 2002, and were analyzed for CO_2 and CO mixing ratios and thereafter for $^{14}CO_2$ by AMS to determine the fossil fuel CO_2 component (compare Figure 5 and discussion below).

[27] REMO modeling results from the lowest vertical box are also displayed in Figure 3 for January 2002. For CO_2 and CO the two different emissions inventories for fossil fuels (EDGAR and IER) have been used with the same setup concerning other CO sources and sinks. For ^{222}Rn a mean soil exhalation rate of 52 Bq m^{-2} h^{-1} (0.72 atom cm^{-2} s^{-1}) was used which corresponds to the recommended value for this latitude according to *Gupta et al.* [2004]. This exhalation rate is slightly lower than the mean value of 57 Bq m^{-2} h^{-1} derived from direct observations in the Heidelberg catchment area, and used in regional studies on trace gas flux estimates, i.e., applying the radon tracer method [*Levin et al.*, 1999].

[28] Both fossil fuel emissions inventories applied in REMO lead to similar CO_2 mixing ratios, but CO mixing ratios show significant differences. However, none of the model runs captures the observations on 5 and 6 January (and also not on 17 and 18 January). Total agreement cannot be expected here because it is unlikely that the height of the actual inversion layer corresponded to the height of the lowest level in the model. It also has to be kept in mind that the measurements were carried out at one point in a 55 km $\times$ 55 km model box, and the catchment area of the measurements was possibly smaller than this box because of low wind speed during the strong inversion situation (Figure 3e). During well mixed atmospheric conditions (second half of January 2002), modeled and observed wind speed and CO_2 mixing ratios agree very well, only CO shows short-term peaks arising during rush hour (e.g., 21–25 January) that are not captured by the model.

[29] For ^{222}Rn the situation is different, here the model results are generally higher than the observations. Since the soil exhalation rate used in the model is slightly smaller compared to our direct observations this would indicate a tendency of the model to underestimate boundary layer mixing and thus overestimate ground level mixing ratios. If this is the case, then CO_2 and CO mixing ratios would be overestimated by the model as well. This would then point to CO_2 and CO emissions in the catchment area of Heidelberg to be larger in reality than quoted in the IER and EDGAR databases and/or that winter time biogenic CO_2 fluxes are underestimated. However, the first half of January 2002 was extremely cold with frozen soil and some permanent snow cover (even) in the Rhine valley. This might have reduced the ^{222}Rn exhalation rate in the area, and could explain the low mixing ratios observed.

[30] Observed and modeled CO_2, CO and ^{222}Rn mixing ratios in August 2002 in Heidelberg are shown in Figure 4 together with wind velocity. Here the model results are significantly higher than the observations for all three gases, mainly during nighttime. In particular modeled ^{222}Rn maxima during nighttime inversion situations are higher by up to 50–100% compared to observations. However, the model very nicely captures the synoptic variability of ^{222}Rn minima as well as the phasing and amplitude of nighttime maxima during moderate wind speed.

[31] For CO, EDGAR emissions always yield higher nighttime mixing ratios than IER emissions, which is due to the missing diurnal cycle in the EDGAR emissions, but in both cases modeled data are 50–100% higher than the observations. As in January, for CO_2 both model estimates compare well with each other, but similar as CO and ^{222}Rn, are higher than the observations. Although the assumed ^{222}Rn soil exhalation rate of 0.72 atoms cm^{-2} s^{-1} is well within the uncertainty range of 20–30% for the catchment area of Heidelberg the REMO model overestimates ^{222}Rn mixing ratios in Heidelberg in winter and in summer. From this we conclude that (vertical) mixing in the nighttime boundary layer is probably underestimated by the model. Therefore we interpret the overestimation of CO_2 and CO mixing ratios by REMO at least in summer as being partly due to the underestimated vertical mixing. To account for this model deficiency, we used the ratio of measured (meas) and modeled (mod) ^{222}Rn activity and applied a correction to

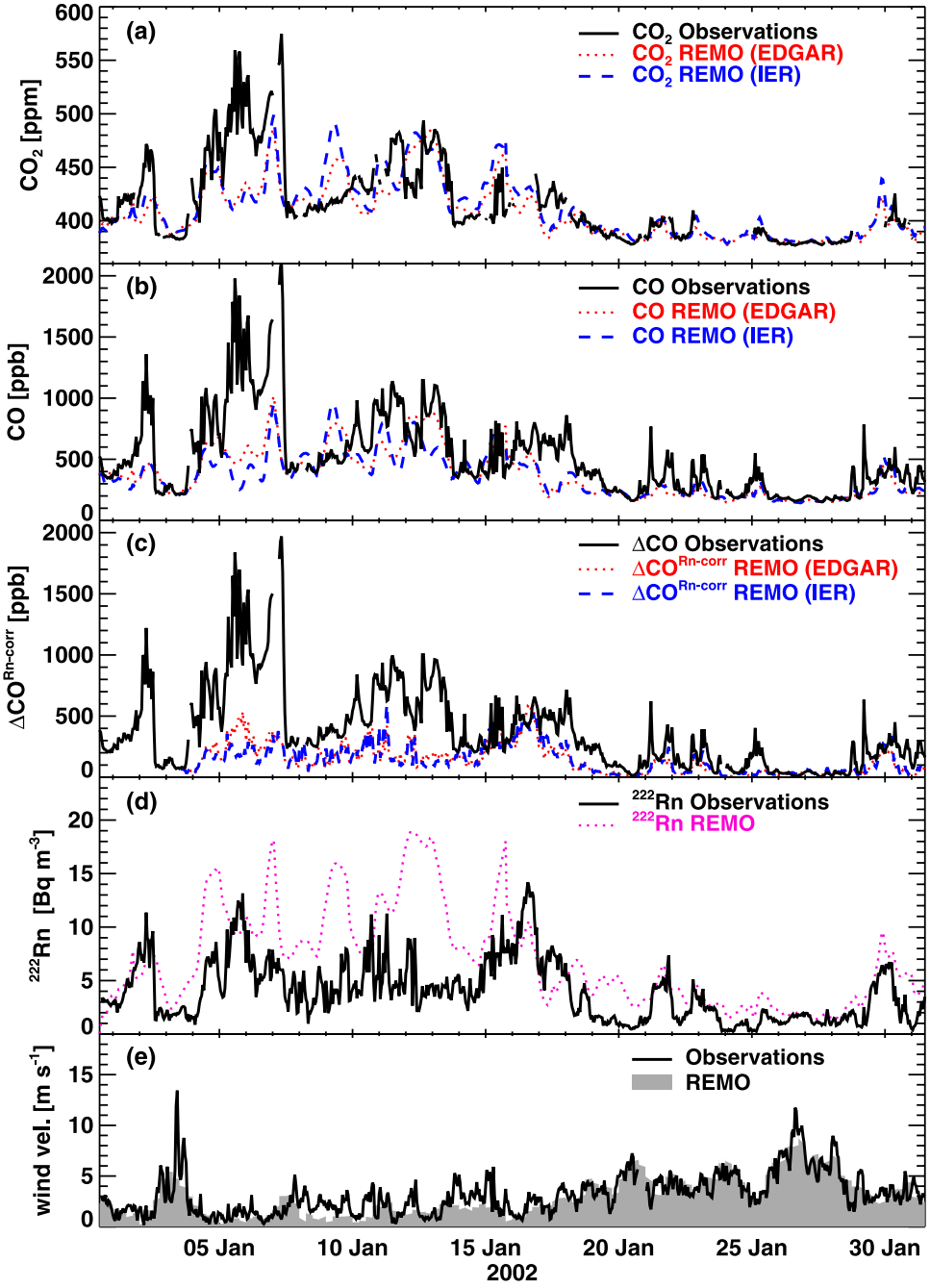

Figure 3. Hourly (a) CO_2 and (b) CO mixing ratios as well as (d) ^{222}Rn activity and (e) wind velocity in Heidelberg in January 2002: comparison of observations with REMO model results. (c) The radon-corrected CO offset from background concentrations is plotted for comparison (see equation (4b)).

the modeled hourly fossil fuel CO_2 and CO offset (compared to background) in Heidelberg according to

$$\Delta CO_2(\text{foss})^{\text{Rn-corr}} = \Delta CO_2(\text{foss})_{\text{mod}} \cdot \frac{^{222}\text{Radon}_{\text{meas}}}{^{222}\text{Radon}_{\text{mod}}} \quad (4a)$$

$$\Delta CO^{\text{Rn-corr}} = \Delta CO_{\text{mod}} \cdot \frac{^{222}\text{Radon}_{\text{meas}}}{^{222}\text{Radon}_{\text{mod}}} \quad (4b)$$

This Rn correction has been applied to all hourly model results, and the effect on ΔCO in January and August 2002 is displayed in Figures 3c and 4c (compare also section 4.5 and Figure 9).

[32] In summary, we conclude that REMO is able to reproduce the general characteristics of continuous Heidelberg trace gas and meteorological observations fairly well. This is an important prerequisite for our assessment.

4.2. Event Samples

[33] Figures 5 and 6 show two typical periods when event samples have been collected: The winter event (Figure 5) was sampled on 4–5 January 2002 at the start of the very

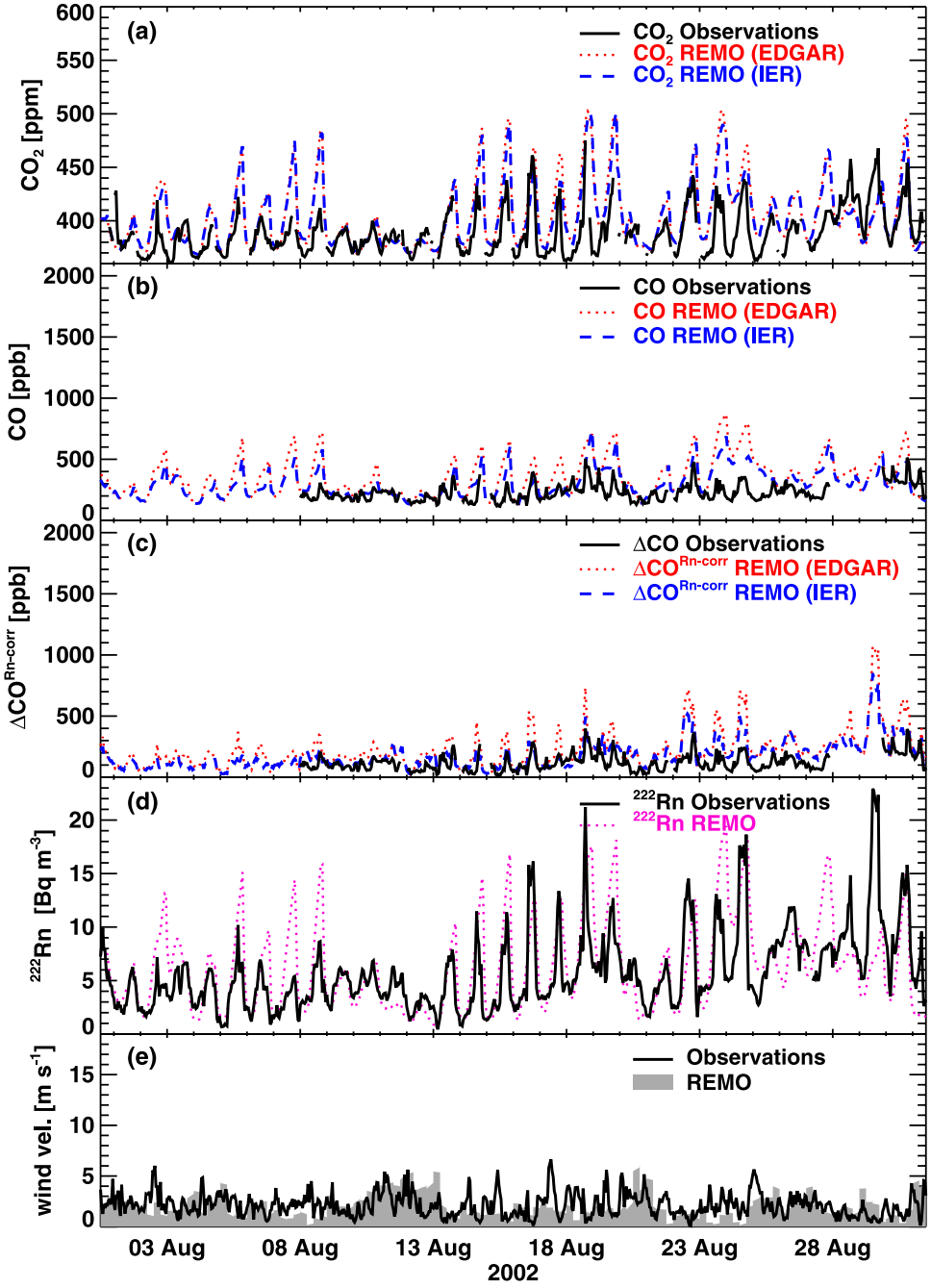

Figure 4. Same as Figure 3, but for August 2002.

strong winter inversion situation already discussed above. The summer event (Figure 6) was collected during the morning of 16 August 2002, when CO increased by about 200 ppb and CO_2 by about 50 ppm above local background during rush hour. The ^{14}C-based fossil fuel CO_2 mixing ratio above the local background (which for events is defined as the mixing ratio (and $^{14}CO_2$ value) at the start time of the event, i.e., the lowest CO_2 mixing ratio and the highest $\Delta^{14}CO_2$ value) is shown in Figures 5c and 5d and 6c and 6d as the grey shaded areas.

[34] During the very cold winter event at the beginning of January 2002, more than 70% of the ΔCO_2 offset compared to background was caused by fossil fuel emissions (local soils were frozen during this period). It is clearly visible in Figures 5a–5c that REMO results underestimate CO_2, CO and also fossil fuel ΔCO_2 during this event. It is possible that the area of source influence for this event was much smaller than the 55 km × 55 km grid box around Heidelberg and that the observed signal is caused by very local and thus high emissions. In Figure 5d we have used the additional information that can be obtained from the continuous CO observations: As all fossil fuel CO_2 emissions are associated with CO emissions, we are able to calculate ΔCO_2(foss) from the ΔCO offset compared to background if we know the CO/CO_2(foss) ratio of these emissions. We took respective information from the emissions inventories

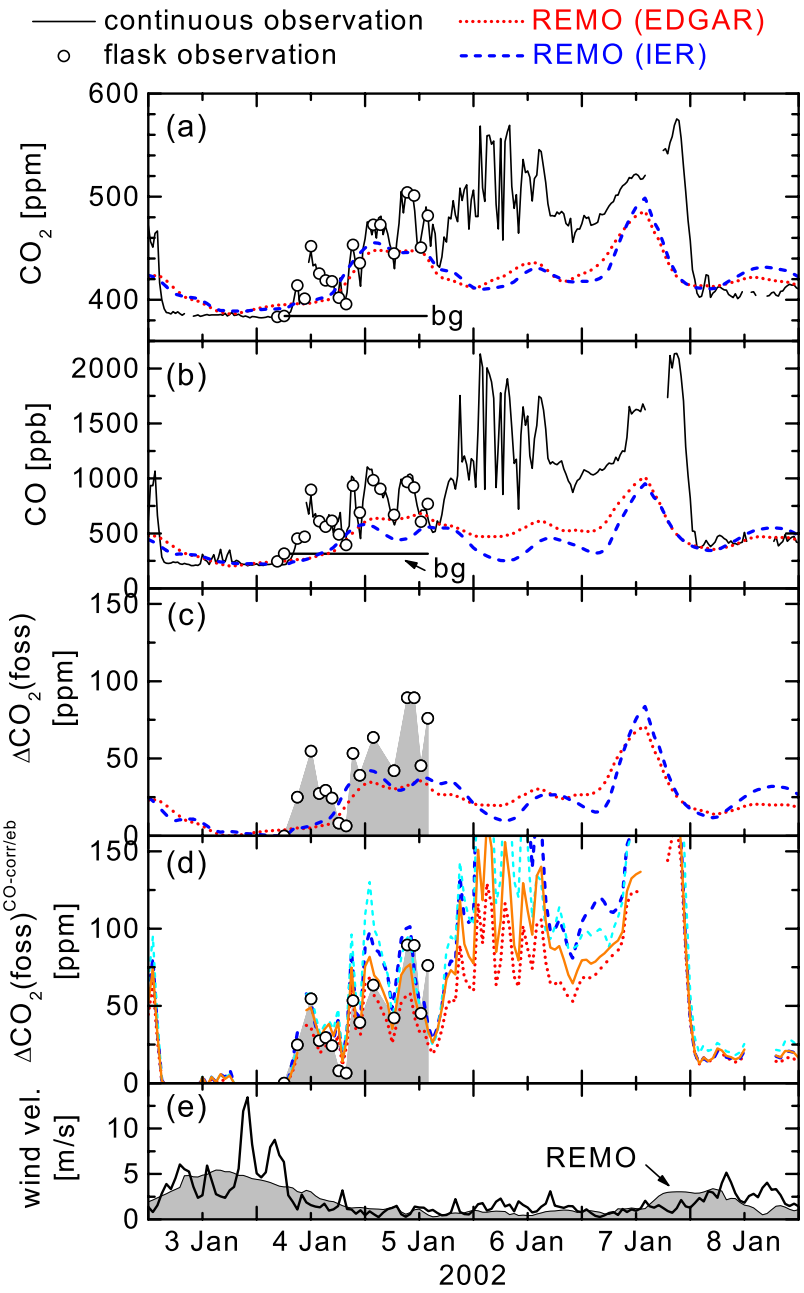

Figure 5. (a) CO_2 and (b) CO mixing ratios for a typical winter event in Heidelberg. Solid lines represent continuous (half-hourly) measurements, open circles represent flask samples, and dotted (EDGAR) and dashed (IER) lines represent hourly model results. (c) Fossil fuel CO_2 component above the local background. The grey shaded area represents the flask observations, and the dotted (EDGAR) and dashed (IER) lines represent REMO model results. (d) Same as Figure 5c but with the modeled CO_2(foss) corrected with the measured ΔCO mixing ratio according to equation (6) ($\Delta CO_2(foss)^{CO\text{-}corr}$, dotted red (EDGAR) and dashed blue (IER) lines). Also plotted is ΔCO_2(foss) estimated from the observed ΔCO mixing ratio and the CO/CO_2(foss) ratio of the emissions inventories according to equation (5) ($\Delta CO_2(foss)^{eb}$, solid orange (EDGAR) and dashed cyan (IER) lines). (e) Wind velocity. The black line represents the observations, and the grey shaded area marks the model estimates.

and assumed that during events the Heidelberg catchment area consists of only the one EDGAR 1° × 1° grid box where the sampling site is located (respectively the corresponding four 50 km × 50 km grid boxes of the IER inventory). We call this the small catchment area. The emissions based $\Delta CO_2(foss)^{eb}$ can then be computed by

$$\Delta CO_2(foss)^{eb} = \Delta CO_{meas} \cdot \frac{CO_2(foss)_{inventory}}{CO_{inventory}} \quad (5)$$

The resulting emission based values are displayed in Figure 5d (Figure 6d for the summer event) as solid

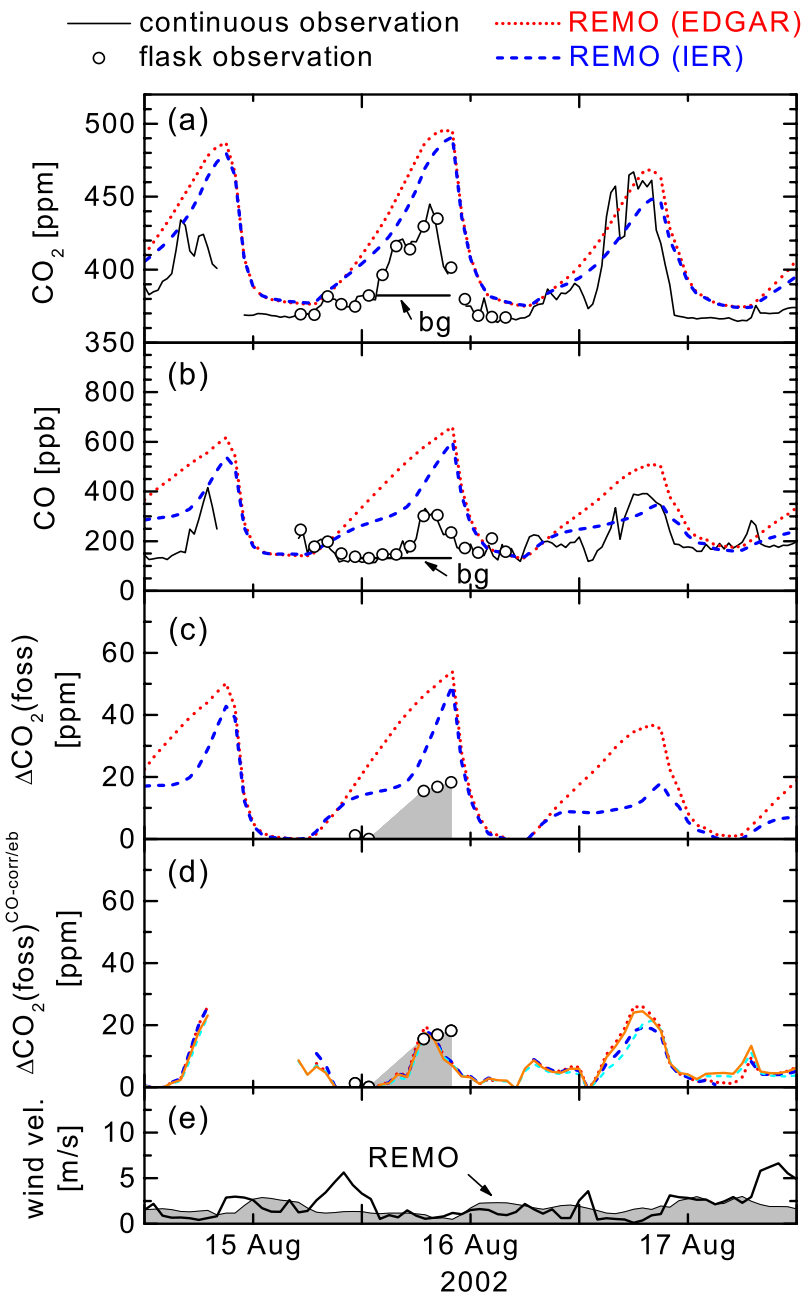

Figure 6. Same as Figure 5, but for a typical summer event.

orange/dashed cyan lines. A respective CO correction was also applied to the modeled $\Delta CO_2(\text{foss})$ according to

$$\Delta CO_2(\text{foss})^{CO-corr} = \Delta CO_2(\text{foss})_{mod} \cdot \frac{\Delta CO_{meas}}{\Delta CO_{mod}} = \Delta CO_{meas} \cdot \frac{\Delta CO_2(\text{foss})_{mod}}{\Delta CO_{mod}} \quad (6)$$

with the resulting data also displayed in Figure 5d (Figure 6d for the summer event) as dotted red/dashed blue lines. The correction of equation (6) serves several purposes: First, it partly corrects for transport errors in the model in a similar way as the ^{222}Rn correction of equations (4a) and (4b); second, it corrects for nonrepresentativeness of the Heidelberg measurements (very local pollution events); and third, it could improve the model results of CO_2(foss) if, for yet unknown reasons, the CO/CO_2(foss) emissions ratios would be more accurately represented in the inventories than the individual CO or CO_2(foss) emissions themselves. Note that equation (6) can be interpreted as deriving $\Delta CO_2(\text{foss})^{CO\text{-}corr}$ from ΔCO observations and the modeled $\Delta CO/\Delta CO_2$(foss) ratio, in analogy to equation (5).

[35] In fact, the agreement between observed and CO-corrected modeled $\Delta CO_2(\text{foss})^{CO\text{-}corr}$ results has considerably improved compared to the original model results (Figure 5c). However, also the agreement between the $\Delta CO_2(\text{foss})^{eb}$ estimate derived only from ΔCO and emissions inventory data of the CO/CO_2(foss) ratio and the ^{14}C-based

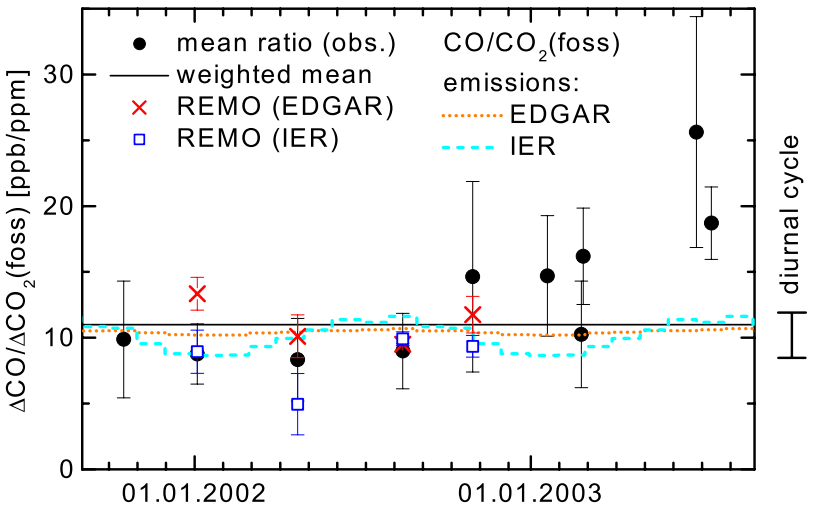

Figure 7. Measured $\Delta CO/\Delta CO_2$(foss) ratios for event samples. Solid circles indicate the mean observed ratio for each of the 10 pollution events, derived from single flask samples as described in the text. The solid line represents the weighted mean from the first 8 events (11.0 ± 1.1 ppb CO/ppm CO_2(foss)). The seasonal cycle of the IER-based emissions ratio (including non-fossil-fuel sources) is plotted as a dashed line (annual mean: 10.1 ppb CO/ppm CO_2(foss)) while the respective emissions ratios from EDGAR are plotted as a dotted line (annual mean: 10.4 ppb CO/ppm CO_2(foss)) (CO/CO_2(foss) inventory data for the small catchment area). Also included are the ratios for the individual events estimated from REMO results (only for 2002).

observations is quite good. While the model estimates automatically take care of the correct catchment area and respective source mix, in the simple $\Delta CO_2(foss)^{eb}$ estimate from ΔCO measurements and emissions inventory data we have to make an assumption about the catchment area that was probably realistic (approximately 1° × 1° box; small catchment area) with respect to the CO/CO_2(foss) ratio.

[36] In the summer event shown in Figure 6 the fossil fuel component was quite small, namely, only about 15 ppm or 30% of the total CO_2 morning peak. As was already visible in Figure 3, in summer for all components REMO overestimates nighttime mixing ratios. Although only a few samples were analyzed for ^{14}C and yielded significant fossil fuel CO_2 in the summer event, it is obvious that the IER-based model results compare slightly better to the observations than the EDGAR results, mainly because they include a diurnal cycle in the emissions, which is not the case for EDGAR. Also in the summer event we corrected the modeled ΔCO_2(foss) according to equation (6), which then yielded very good agreement of $\Delta CO_2(foss)^{CO\text{-}corr}$ with the observations (Figure 6d). Again, also the simple extrapolation of $\Delta CO_2(foss)^{eb}$ from ΔCO and emissions inventory data yields similarly good agreement with the observed ΔCO_2(foss).

[37] Generally, it was very difficult to "catch" strong pollution events in Heidelberg in summer, because mean CO offsets were only on the order of 100 ppb. Still, in total 10 pollution events were collected and analyzed during this study, three during summer and 7 during spring, autumn and winter. For a single event, up to 16 flask samples have been collected and analyzed for CO_2, CO and $^{14}CO_2$.

4.3. $\Delta CO/\Delta CO_2$(foss) Ratios From Events

[38] For every single sample in every pollution event, the ratio $\Delta CO/\Delta CO_2$(foss) between the measured ΔCO mixing ratio in the flasks and the ^{14}C-based fossil fuel CO_2 was determined. To calculate the mean $\Delta CO/\Delta CO_2$(foss) ratio for an event, only samples with ΔCO_2(foss) significantly (more than 2 standard deviations) larger than zero were taken into account. The mean $\Delta CO/\Delta CO_2$(foss) ratios for all events are displayed in Figure 7 (solid circles). The error bars are the standard deviations of the individual ratios within one event. In the two events in summer 2003 only one flask sample each showed a significant ΔCO_2(foss). Here the error bar represents the uncertainty arising from measurement uncertainty. These two events had been sampled during rush hour and represent very local conditions, which most probably differ from the mean conditions in the Heidelberg grid box. These samples have thus not been included in the weighted mean $\Delta CO/\Delta CO_2$(foss) ratio for the events. The weighted mean for the remaining eight events of this study yielded (11.0 ± 1.1) ppb CO/ppm CO_2(foss). It has been calculated by weighting the ratio from each event with the number of flask samples included in the calculation of the mean ratio of this event. Besides the measurements we also plotted in Figure 7 the ratios estimated from REMO results for the times of the events using EDGAR and IER emissions. Error bars have been calculated in the same way as for the observations.

[39] Also included in Figure 7 are the EDGAR and IER emission inventory ratios for the respective box(es) around Heidelberg, including their seasonal and diurnal cycle (IER inventory) as well as non-fossil-fuel CO sources. Annual mean emissions ratios are 10.4 ppb CO/ppm CO_2(foss) for EDGAR and 10.1 ppb CO/ppm CO_2(foss) for IER. The temporal variation in the emission ratio of IER is caused by temporally varying contributions from different sources, which have different CO/CO_2 emission ratios. For example, the CO/CO_2 emission ratio for road transport is more than 1

order of magnitude larger than the ratio for domestic heating. Thus, if, e.g., the contribution of traffic increases in the total fossil fuel source, as is the case in summer, the average CO/CO_2 emission ratio for fossil fuels will also increase.

[40] The measured $\Delta CO/\Delta CO_2$(foss) ratios do not directly reflect the seasonal cycle of the emissions. Taking into account that the amplitude of diurnal variations in the emissions ratio (shown as vertical bar at the right axis of Figure 7) is of similar size as the amplitude of seasonal variations, this seems not surprising. However, the temporal variation in the observed $\Delta CO/\Delta CO_2$(foss) ratio during the course of a day does not coincide with the diurnal cycle in the emission ratio derived from the IER inventory (data not shown). Moreover, the errors of the mean ratio of an event illustrate the high variability of the observed atmospheric $\Delta CO/\Delta CO_2$(foss) ratio within only a few hours. The weighted mean of the emissions ratios derived from REMO simulations for the events in 2002 yielded (11.8 ± 0.9) ppb CO/ppm CO_2(foss) (EDGAR) and (8.9 ± 1.1) ppb CO/ppm CO_2(foss) (IER), compared to measured (9.5 ± 1.2) ppb CO/ppm CO_2(foss) for the event samples collected in 2002. Thus applying REMO is not a substantial improvement compared to the direct emissions ratios only and selecting the correct catchment area of the Heidelberg station with a (coarse resolution) model like REMO is obviously not important for event situations. Also the similar course of $\Delta CO_2(foss)^{eb}$ (equation (5)) and $CO_2(foss)^{CO\text{-}corr}$ (equation (6)) in Figures 5d and 6d indicates that including REMO and processes associated with atmospheric chemistry does not improve the estimate of ΔCO_2(foss). This is probably due to the fact that by accident the hydrocarbon oxidations source of CO is almost balanced by the photochemical CO sink and the soil deposition sink. However, if we would, in addition, neglect the non-fossil-fuel emissions this would decrease the emissions ratios by 17% (EDGAR) and 24% (IER) and lead to significantly smaller ratios than observed. This shows that in general non-fossil-fuel CO emissions, VOC production and soil uptake need to be considered when attempting to use CO as a quantitative tracer for fossil fuel CO_2.

4.4. CO_2, CO, and $^{14}CO_2$ Results From Integrated Sampling

[41] Two-weekly/weekly integrated $^{14}CO_2$ measurements in Heidelberg are shown in Figure 8a in comparison to background air. The $^{14}CO_2$ background was derived from Jungfraujoch measurements, which generally compare very well with marine background air observations [*Levin and Kromer*, 2004; I. Levin, unpublished Heidelberg data, 2003, 2004]. The $\Delta^{14}CO_2$ level in Heidelberg is always lower than at Jungfraujoch with depletions in winter of up to 60‰. These $\Delta^{14}C$ depletions translate into two-weekly/weekly mean fossil fuel CO_2 mixing ratios (as calculated according to equation (3)) of up to 25 ppm (Figure 8b). Figure 8c shows the mean ΔCO offsets compared to background for the same intervals. The CO background at 49.4°N was calculated in analogy to Globalview CO_2 (K. Masarie, personal communication, 2004) and was extrapolated for the period of December 2003 to April 2004. A strong correlation between ΔCO and ^{14}C-based regional fossil fuel CO_2 is already visible from comparison of Figures 8b and 8c.

[42] The $\Delta CO/\Delta CO_2$(foss) ratios for the individual integrated CO_2 samples are displayed in Figure 8d. Only samples with more than 60% of the sampling time covered with continuous measurements of ambient CO_2 and CO mixing ratios and with a significant amount of ΔCO_2(foss) (more than two standard deviations from zero) have been taken into account. From the 66 samples collected between September 2001 and April 2004 an error weighted mean $\Delta CO/\Delta CO_2$(foss) ratio with weekly samples weighted with the factor 0.5 compared to two-weekly integrated samples was calculated to (12.2 ± 0.4) ppb CO/ppm CO_2(foss). This ratio is slightly higher than the mean ratio derived from the event samples of (11.0 ± 1.1) ppb CO/ppm CO_2(foss). This can be explained by different catchment areas for the integrated and event samples: While typical event situations are only observed during inversion situations at low wind speed, which implies only a small catchment area, the integrated samples were collected during all nights and include also situations with high wind speed and a catchment area of up to several hundred km radius around the sampling site.

[43] The catchment area for the integrated samples was approximated as an area around Heidelberg that was hit by more than 75% of all 24 hours back trajectories arriving at the sampling site. It covers an area of 11 EDGAR grid boxes around the sampling site with emphasis on the southwest direction, according to the mean wind direction. Mean emissions ratios were calculated from inventory data for this "large" catchment area, and the respective values, including also nonfossil CO emissions, are plotted in Figure 8d in comparison to the observations. Annual mean emissions ratios are 12.7 ppb CO/ppm CO_2(foss) for EDGAR and 13.1 ppb CO/ppm CO_2(foss) for IER (only nighttime values). These emissions ratios for the large catchment area are about 25% larger than for the small catchment area of the events (see also Figure 2) and thus should lead to larger atmospheric $\Delta CO/\Delta CO_2$(foss) ratios in the integrated samples, which is in general agreement with the observations. The mean values of the emissions based CO/CO_2(foss) ratios both compare well with the mean of the observations to better than ±10%.

4.5. Comparison of Integrated Samples With 2002 REMO Results

[44] For the same time periods of approximately 2 weeks as in the integrated observations mean nighttime values at Heidelberg have been extracted from REMO simulations for 2002. Background values were taken from the modeling results in an analogue way as for the measurements. The results are shown in Figure 9 together with the observed 2002 values. In order to reduce model transport uncertainties and hence allow a more quantitative evaluation of emissions inventories, ΔCO as well as regional fossil fuel CO_2 from both simulations (REMO(EDGAR) and REMO(IER)) were corrected according to equations (4a) and (4b) using ^{222}Rn. While for $\Delta CO_2(foss)^{Rn\text{-}corr}$ both emissions inventories for most of the time give similar results, $\Delta CO^{Rn\text{-}corr}$ in summer and autumn are significantly larger for the EDGAR inventory than for IER. However, most important, with both emissions inventories modeled

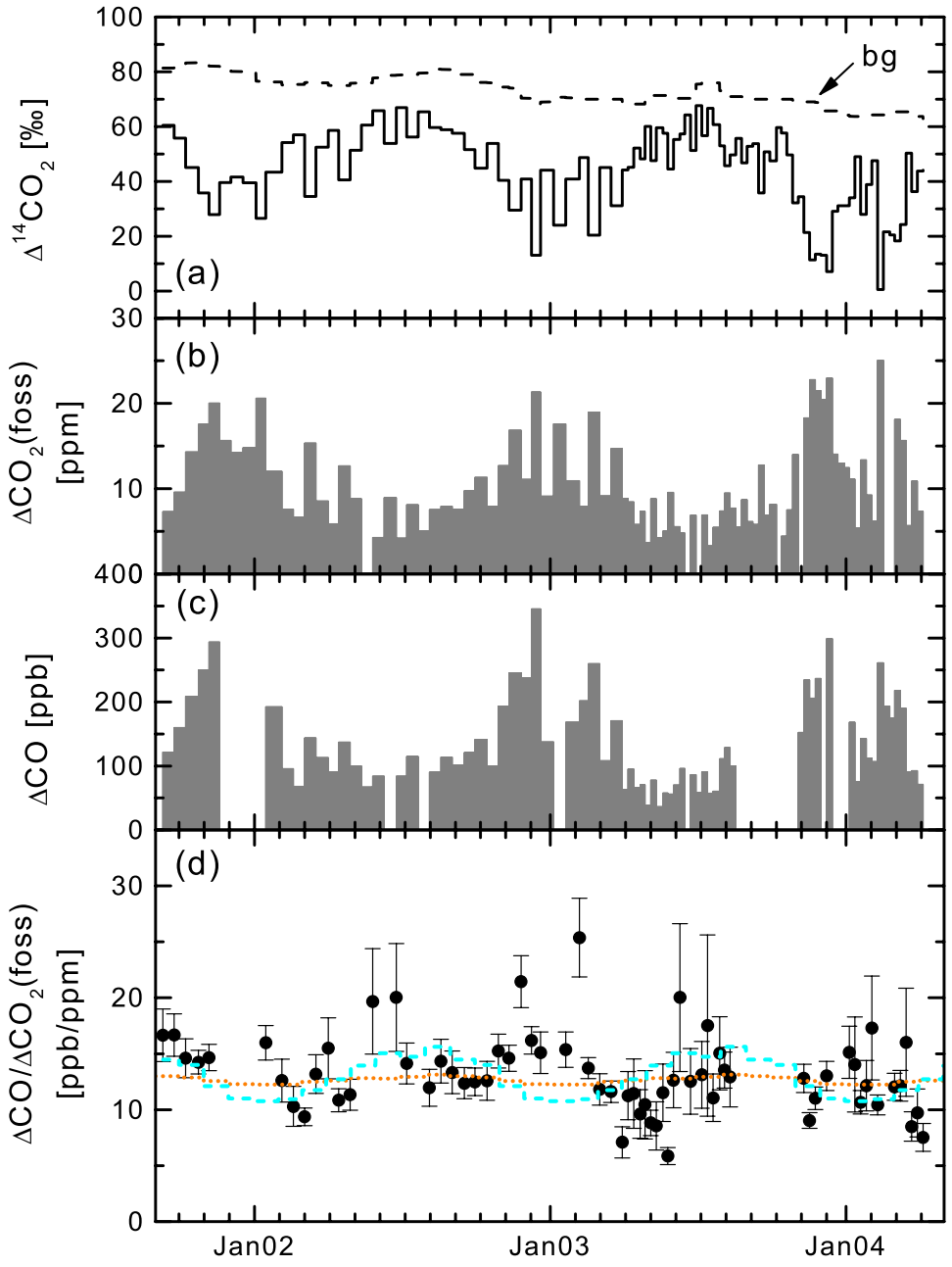

Figure 8. (a) Two-weekly/weekly integrated nighttime $\Delta^{14}CO_2$ in Heidelberg (solid line) in comparison with the background level at Jungfraujoch (dashed line). (b) ^{14}C-based fossil fuel CO_2 and (c) mean ΔCO offset relative to background for the sampling intervals. (d) $\Delta CO/\Delta CO_2$(foss) ratios for individual samples collected from September 2001 to April 2004 including error bars (mean: (12.2 ± 0.4) ppb CO/ppm CO_2(foss)). For comparison, the seasonal cycle of the IER-based emissions ratio (including non-fossil surface CO emissions) is plotted as a dashed line (annual mean: 13.1 ppb CO/ppm CO_2(foss)) while the respective ratio from EDGAR is plotted as a dotted line (annual mean: 12.7 ppb CO/ppm CO_2(foss)) (CO/CO_2(foss) inventory data for the large catchment area).

ΔCO and regional fossil fuel CO_2 offsets compared to background air are higher than the observations, particularly in summer and autumn (but slightly lower in winter, December, January, February). As the model results have already been largely corrected for transport deficiencies by ^{222}Rn, and the uncertainty in the measured fossil fuel CO_2 component is smaller than 3 ppm for individual samples, the disagreement between model and observations in summer and autumn is most probably caused by errors in the inventories.

[45] Figure 9c shows the $\Delta CO/\Delta CO_2$(foss) ratio (a result which is largely independent from the transport in the model) in comparison with observations. Here for most of the time the REMO results based on IER emissions yield

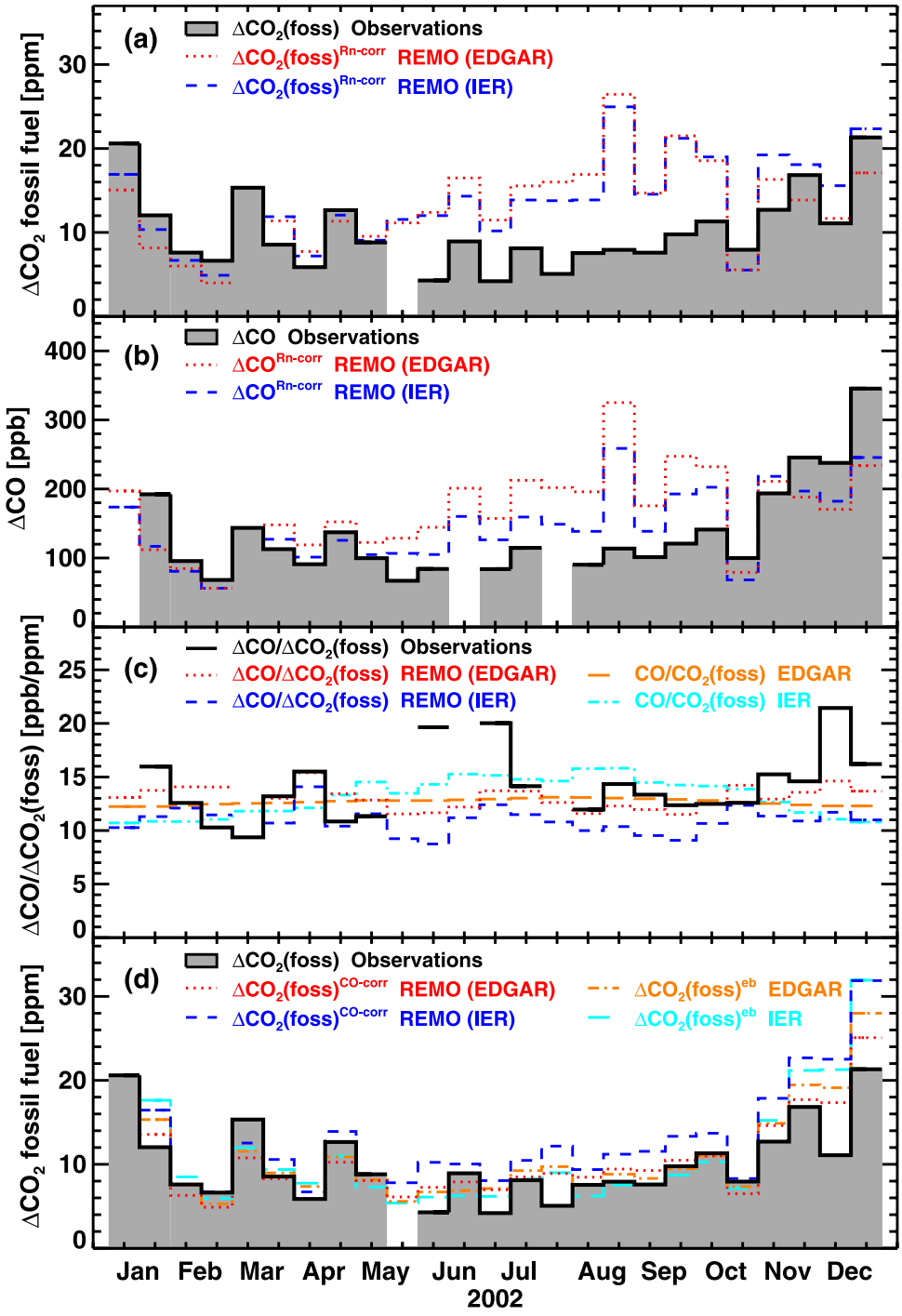

Figure 9. (a) ΔCO_2(foss), (b) ΔCO, and (c) the respective $\Delta CO/\Delta CO_2$(foss) ratio of the two-weekly integrated samples in comparison to the REMO results using IER- and EDGAR-based emissions inventories. (Observed ratios have not been plotted and included in the mean values for samples where the fossil fuel CO_2 component was not significant or less than 60% of the sampling time was covered with continuous mixing ratio measurements.) ΔCO_2(foss) (Figure 9a) and ΔCO (Figure 9b) model results have been ^{222}Rn corrected according to equations (4a) and (4b). (d) Comparison of observed ΔCO_2(foss) and ΔCO_2(foss) estimated from ΔCO observations according to equation (5) as well as model estimates that had been corrected with observed ΔCO according to equation (6).

about 20% smaller ratios than those based on EDGAR emissions. A significant seasonal cycle can neither be observed in the measurements nor in any of the two model simulations. Compared to the ratio derived directly from emissions of the large catchment area, summer REMO (IER) values are always lower by about 30%. The difference between direct EDGAR emissions ratios and REMO (EDGAR) results is not significant (see Table 1). Finally, Figure 9d

Table 1. $\Delta CO/\Delta CO_2(foss)$ Ratios and $\Delta CO_2(foss)^{CO\text{-}corr/eb}$ [a]

	Ratio	$\Delta CO_2(foss)^{CO\text{-}corr/eb}$		
	Mean 2002,[b] ppb/ppm	Mean 2002, ppm	Bias, ppm	RMS, %
Observations	13.5 ± 2.5	11.4	–	–
ΔCO, $\Delta CO_2(foss)$ REMO (EDGAR)	13.0 ± 0.9	11.9	0.5	18.1
ΔCO, $\Delta CO_2(foss)$ REMO (IER)	11.5 ± 1.1	14.2	2.8	35.8
ΔCO, $\Delta CO_2(foss)$ REMO (EDGAR) without deposition	14.2 ± 0.8	11.0	−0.4	16.7
ΔCO, $\Delta CO_2(foss)$ REMO (IER) without deposition	12.6 ± 1.1	13.1	1.7	29.5
CO, $CO_2(foss)$ emissions-based (EDGAR)	12.7 ± 0.3	12.5	1.1	24.2
CO, $CO_2(foss)$ emissions-based (IER)	13.1 ± 1.6	12.9	1.5	36.1

[a] $\Delta CO/\Delta CO_2(foss)$ ratios from observations compared to REMO results with and without soil deposition together with observed (^{14}C-based) $\Delta CO_2(foss)$ and REMO-simulated $\Delta CO_2(foss)^{CO\text{-}corr}$ corrected with measured ΔCO according to equation (6). Also given are $\Delta CO_2(foss)^{eb}$ values estimated from observed ΔCO and $CO/CO_2(foss)$ values from inventory data according to equation (5). For the observations the error weighted mean of the individual integrated samples in 2002 is given; for the REMO results and $\Delta CO_2(foss)^{eb}$ data the same weights have been applied. For $\Delta CO_2(foss)^{CO\text{-}corr/eb}$ also the deviation of the weighted mean compared to the observations and the root-mean-square (RMS) value of the deviations compared to the observations of individual samples is listed.

[b] Plus or minus standard deviation.

shows the REMO results of $\Delta CO_2(foss)^{CO\text{-}corr}$ from both inventories corrected by the continuous ΔCO observations according to equation (6) in comparison to observations as well as estimated $\Delta CO_2(foss)^{eb}$ values derived only from inventory data according to equation (5). The weighted mean values of the ratios and of measured and modeled $\Delta CO_2(foss)$ for the integrated samples in 2002 are summarized in Table 1.

[46] For both inventories the REMO $\Delta CO/\Delta CO_2(foss)$ ratios compare much better to the observed ratios than the ΔCO and $\Delta CO_2(foss)$ offsets themselves. In the case of IER emissions the REMO-derived ratio is significantly smaller than the observations while the mean REMO (EDGAR) ratio and that derived from both emissions inventories only (large catchment area) compare well with the observed atmospheric ratio. This is surprising at a first glance, however, the low IER-based ratio derived from REMO can be explained by a very low $CO/CO_2(foss)$ emissions ratio in the 50 km × 50 km IER grid cell which contributes most to the emissions in the grid cell of the 0.5° × 0.5° rotated REMO grid in which Heidelberg is located. This very low emissions ratio is caused by large industrial emissions about 20 km northwest of Heidelberg, and does not show up as an extreme in the 1° × 1° EDGAR grid of Heidelberg and even less in the mean value for the large catchment area. This finding tells us that the model simulations during nighttime are obviously too strongly influenced by these local emissions. Hence one has to carefully inspect the heterogeneity of emissions in the immediate neighborhood of a sampling station when interpreting these measurements with a regional model of limited spatial resolution.

[47] For 2002 the modeled $\Delta CO_2(foss)$ corrected with CO observations according to equation (6), $\Delta CO_2(foss)^{CO\text{-}corr}$, is larger compared to the observed $\Delta CO_2(foss)$ based on ^{14}C by 4% using EDGAR and by 25% using IER emissions with a root-mean-square deviation (RMS) of 18% (EDGAR) and 36% (IER). The RMS value for the EDGAR inventory is smaller than for IER because in November, December and January, when $\Delta CO_2(foss)$ and thus the weighting of these samples is high, REMO (EDGAR) is closer to the observations than REMO (IER). On the other hand, $\Delta CO_2(foss)^{eb}$ estimated from the emissions inventories according to equation (5) are slightly higher than the observations but in the same range as the ΔCO corrected REMO results. Obviously, averaging over two weeks can smooth heterogeneities of emissions, and at this temporal resolution can yield comparable results to those estimated by a model like REMO. Table 1 also shows REMO (EDGAR) and REMO (IER) results when calculating CO mixing ratios excluding the soil deposition/oxidation sink. As expected, modeled ΔCO mixing ratios are higher in this simulation (by about 10%) than in the standard run. Neglecting both, the VOC oxidation source and the soil deposition sink yields results only slightly (<5%) different from the standard run but with a slightly larger RMS error (data not shown). Both terms in the CO budget, VOC oxidation and soil deposition are highly uncertain (about 50–100%), and, besides the errors in the inventory data which are very difficult to estimate, thus add another about 20% to the total uncertainty of CO-based fossil fuel CO_2.

5. Conclusions

[48] Continuous CO_2, CO and ^{222}Rn observations in Heidelberg supplemented by high-precision $^{14}CO_2$ measurements provided new insight into the value of carbon monoxide as a quantitative tracer for fossil fuel CO_2. Additional regional model simulations with REMO provided estimates of CO_2 and other trace substances transported from ground level sources to the Heidelberg sampling site. Underestimation of vertical transport in REMO during calm nights could partly be corrected for by using the observed and modeled ^{222}Rn activity, thus providing more reliable radon-corrected model estimates of the regional fossil fuel CO_2 offset and total ΔCO based on emissions inventories and additional source/sink information. The following questions could be addressed in detail.

5.1. Can We Verify/Falsify Fossil Fuel CO_2 and CO Emissions Inventories in the Catchment Area of Heidelberg?

[49] Our radon-corrected model estimates of $\Delta CO_2(foss)$ and ΔCO turned out to be higher by up to a factor of 2 in summer and autumn, and lower by 20–30% in winter, compared to the observations. In the case of CO, nonfossil emissions contribute about 20% and CO production by

VOC oxidation (mainly in summer) another 10% to the total modeled offset with uncertainties of these contributions on the order of 50–100%. Despite the uncertainties in CO model estimates, the overestimation of ΔCO_2(foss) and also ΔCO in the summer and autumn months is significant and must be due to overestimation of emissions in the EDGAR and IER inventories. This is an important finding of our study. However, our analysis also clearly shows that the atmospheric CO mixing ratio, even in a polluted area such as Heidelberg, besides fossil fuel emissions, is largely determined by a number of highly uncertain processes, which have the potential to individually change the ΔCO offset by up to 20%. This is a strong drawback of any attempt to use CO as a quantitative tracer to estimate fossil fuel CO_2.

5.2. Can We Use Our Observations to Verify/Falsify CO/CO_2(foss) Ratios of Emissions?

[50] Although the fossil fuel CO_2 and CO emissions in both inventories seem to be too large in summer and autumn in the Heidelberg catchment area, the mean CO/CO_2(foss) ratio derived from inventories, when transported by REMO and when also taking into account CO production from VOCs, agrees surprisingly well with the observations to within ±17% RMS error for the EDGAR inventory and ±23% RMS error for IER. The reason why CO/CO_2(foss) ratios compare much better with observations than ΔCO and ΔCO_2(foss) alone still needs to be investigated. Particularly important will be to find out if this is correct only for the Heidelberg catchment area or also in other regions of Europe.

5.3. Can Continuous CO Observations Improve Our Estimates of Regional Fossil Fuel CO_2 at a Continental Station?

[51] At a first glance it seems that using CO measurements to quantify regional fossil fuel CO_2 at a continental site would introduce more uncertainty than constraints. However, in our study we could show that using the high-resolution CO measurement as a normalization tool to correct for model deficiencies as well as deficiencies in the emissions inventories could largely improve the agreement between observed and modeled ΔCO_2(foss). However, note that this was possible mainly because the mean CO/CO_2(foss) ratios of the emissions inventories in the Heidelberg catchment area were more or less correct.

5.4. Do We Need a Regional Model (Such as REMO) to Determine ΔCO_2(foss) With ΔCO From Inventory Data?

[52] For small-scale event situations where the mean catchment area consists of just one grid cell around the sampling site the application of REMO will not significantly improve the accuracy of the determination of the fossil fuel CO_2 component, and a direct estimation from CO observations and CO/CO_2(foss) emissions ratios can provide reliable results (but see also 5.3). The same may be true for a sampling site with very homogeneous CO/CO_2(foss) ratios of emissions in the catchment area. For integrated samples which have a larger catchment area than one grid cell of the underlying emissions inventory, a regional model such as REMO can help to properly define the catchment area for every measurement in time, thus providing the correct mix of emissions from different grid points. Also, in less polluted areas the relative influence of CO production by VOCs and of the soil sink increase, which can only be taken care of by a model. Therefore a regional model will be needed to disentangle the regional fossil fuel CO_2 component from a continuous CO_2 record at most continental measurement sites.

5.5. What Would Be the Ideal Observational Network for an Adequate Determination of the Fossil Fuel CO_2 Component?

[53] It is very obvious from our study that for quantifying fossil fuel CO_2 over Europe one should not rely on the available emissions inventories alone, at least in our study area. However, if the ratios of fossil fuel CO_2 and CO emissions are reliable in the inventories, CO observations can successfully be used to determine ΔCO_2(foss) with an uncertainty of about 20–35%. In principle, the application of a regional model allows one to include other processes influencing CO mixing ratios and can further improve the ability to account for the heterogeneity of emissions. However, errors associated with uncertainties in model transport and representativeness of local observations can additionally complicate the interpretation and applicability of the model results. Taking advantage of CO observations can correct the model output for some shortcomings related to transport and other processes that are unaccounted for. Nevertheless, it will be essential to validate CO_2(foss) estimates with $^{14}CO_2$ observations at any continental CO_2 measurement site that is also significantly influenced by fossil fuel emissions. For this purpose, weekly flask sampling will not be sufficient, as it can only provide a snapshot of a particular situation and does not give the complete picture; this can only be provided by integrated sampling. Continuous CO observations can help to derive a higher temporal resolution once the mean fossil fuel CO_2 component is determined by $^{14}CO_2$ measurements, and the mean CO/CO_2(foss) ratio of emissions inventories has been validated. As the CO/CO_2 ratios of important fossil fuel sources will probably change significantly in the future, ongoing $^{14}CO_2$ observations will be indispensable.

[54] **Acknowledgments.** We wish to thank Frank Meinhardt from the German Umweltbundesamt, Schauinsland, for calibrating our CO standards. Ken Masarie (NOAA-CMDL, Boulder, Colorado) provided us with a marine reference curve to define the CO background for Heidelberg. Yvonne Scholz and Stefan Reis (IER, University of Stuttgart, Germany) discussed IER emissions inventory data with us. U.K. would like to thank Galina Churkina and Christian Rödenbeck (MPI for Biogeochemistry, Jena, Germany) for providing simulation results from BIOME-BGC and TM3, respectively, and Martin Schultz (MPI for Meteorology, Hamburg, Germany) for making available the MOZART simulation results. Finally, we want to thank the two anonymous reviewers for their very helpful comments and suggestions to improve REMO CO estimates and the whole manuscript. This work was funded by the European Union under contracts EVK2-CT-1999-00013 (AEROCARB) and GOCE-CT2003-505572 (CarboEurope-IP).

References

Bakwin, P. S., D. F. Hurst, P. P. Tans, and J. W. Elkins (1997), Anthropogenic sources of halocarbons, sulfur hexafluoride, carbon monoxide, and methane in the southeastern United States, *J. Geophys. Res.*, *102*, 15,915–15,925.

Brasseur, G. P., D. A. Hauglustaine, S. Walters, P. J. Rasch, J.-F. Müller, C. Granier, and X. X. Tie (1998), MOZART, a global chemical transport

model for ozone and related chemical tracers: 1. Model description, *J. Geophys. Res.*, *103*, 28,265–28,289.

Brenninkmeijer, C. A. M., C. Koeppel, T. Röckmann, D. S. Scharffe, M. Bräunlich, and V. Gros (2001), Absolute measurement of the abundance of atmospheric carbon monoxide, *J. Geophys. Res.*, *106*, 10,003–10,010.

Chevillard, A., et al. (2002a), Transport of ^{222}Rn using the regional model REMO: A detailed comparison with measurements over Europe, *Tellus, Ser. B*, *54*, 850–871.

Chevillard, A., U. Karstens, P. Ciais, S. Lafont, and M. Heimann (2002b), Simulation of atmospheric CO_2 over Europe and western Siberia using the regional scale model REMO, *Tellus, Ser. B*, *54*, 872–894.

Churkina, G., J. Tenhunen, P. Thornton, E. M. Falge, J. A. Elbers, M. Erhard, T. Grünwald, A. S. Kowalski, Ü. Rannik, and D. Sprinz (2003), Analyzing the ecosystem carbon dynamics of four European coniferous forests using a biogeochemistry model, *Ecosystems*, *6*, 168–184.

de Jong, A. F. M., and W. G. Mook (1982), An anomalous Suess effect above Europe, *Nature*, *298*, 641–644.

Friedrich, R., and S. Reis (Eds.) (2004), *Emissions of Air Pollutants: Measurements, Calculations and Uncertainties–Results From the EUROTRAC Subproject GENEMIS*, 335 pp., Springer, New York.

Friedrich, R., et al. (2003), Temporal and spatial resolution of greenhouse gas emissions in Europe, CarboEurope GHG report, workshop 3, 36 pp., CarboEurope IP, Viterbo, Italy.

Gamnitzer, U. (2003), Accounting for carbon dioxide emissions in the Heidelberg region using atmospheric CO_2, $^{14}CO_2$ and CO measurements (in German), diploma thesis, Univ. Heidelberg, Heidelberg, Germany.

Gerbig, C., S. Schmitgen, D. Kley, and A. Volz-Thomas (1999), An improved fast-response vacuum-UV resonance fluorescence CO instrument, *J. Geophys. Res.*, *104*, 1699–1704.

Greschner, B. (1995), Gas chromatographic measurement of the atmospheric carbon dioxide, methane and N_2O concentration in Heidelberg (in German), thesis, Univ. Heidelberg, Heidelberg, Germany.

Guenther, A., C. N. Hewitt, T. Pierce, B. Lamb, P. Harley, and R. Fall (1995), A global model of natural volatile organic compound emissions, *J. Geophys. Res.*, *100*, 8873–8892.

Gupta, M. L., A. R. Douglass, R. Kawa, and S. Pawson (2004), Use of radon for evaluation of atmospheric transport models: Sensitivity to emissions, *Tellus, Ser. B*, *56*, 404–412.

Hao, W. M., and M.-H. Liu (1994), Spatial and temporal distribution of tropical biomass burning, *Global Biogeochem. Cycles*, *8*, 495–503.

Hauglustaine, D. A., F. Hourdin, L. Jourdain, M.-A. Filiberti, S. Walters, J.-F. Lamarque, and E. A. Holland (2004), Interactive chemistry in the Laboratoire de Météorologie Dynamique general circulation model: Description and background tropospheric chemistry evaluation, *J. Geophys. Res.*, *109*, D04314, doi:10.1029/2003JD003957.

Heimann, M., and S. Körner (2003), The global atmospheric tracer model TM3, *Tech. Rep. 5*, 131 pp., Max-Planck-Inst. für Biogeochem., Jena, Germany.

Horowitz, L. W., S. Walters, D. L. Mauzerall, L. K. Emmons, P. J. Rasch, C. Granier, X. Tie, J.-F. Lamarque, M. G. Schultz, and G. P. Brasseur (2003), A global simulation of tropospheric ozone and related tracers: Description and evaluation of MOZART, version 2, *J. Geophys. Res.*, *108*(D24), 4784, doi:10.1029/2002JD002853.

Jacob, D. (2001), A note to the simulation of the annual and inter-annual variability of the water budget over the Baltic Sea drainage basin, *Meteorol. Atmos. Phys.*, *77*, 61–73.

Karstens, U., R. Nolte-Holube, and B. Rockel (1996), Calculation of the water budget over the Baltic Sea catchment area using the regional forecast model REMO for June 1993, *Tellus, Ser. A*, *48*, 684–692.

Kromer, B., and K. O. Münnich (1992), CO_2 gas proportional counting in radiocarbon dating: Review and perspective, in *Radiocarbon After Four Decades*, edited by R. E. Taylor, A. Long, and R. S. Kra, pp. 184–197, Springer, New York.

Langmann, B. (2000), Numerical modelling of regional scale transport and photochemistry directly together with meteorological processes, *Atmos. Environ.*, *34*, 3585–3598.

Langmann, B., and A. Heil (2004), Release and dispersion of vegetation and peat fire emissions, *Atmos. Chem. Phys.*, *4*, 2145–2160.

Langmann, B., S. E. Bauer, and I. Bey (2003), The influence of the global photochemical composition of the troposphere on European summer smog, part I: Application of a global to mesoscale model chain, *J. Geophys. Res.*, *108*(D4), 4146, doi:10.1029/2002JD002072.

Lawrence, M. G., P. J. Crutzen, P. J. Rasch, B. E. Eaton, and N. M. Mahowald (1999), A model for studies of tropospheric photochemistry: Description, global distributions, and evaluation, *J. Geophys. Res.*, *104*, 26,245–26,277.

Levin, I., and V. Hesshaimer (2000), Radiocarbon: A unique tracer of global carbon cycle dynamics, *Radiocarbon*, *42*, 69–80.

Levin, I., and B. Kromer (2004), The tropospheric $^{14}CO_2$ level in mid-latitudes of the Northern Hemisphere (1959–2003), *Radiocarbon*, *46*, 1261–1272.

Levin, I., K. O. Münnich, and W. Weiss (1980), The effect of anthropogenic CO_2 and ^{14}C sources on the distribution of $^{14}CO_2$ in the atmosphere, *Radiocarbon*, *22*, 379–391.

Levin, I., J. Schuchard, B. Kromer, and K. O. Münnich (1989), The continental European Suess effect, *Radiocarbon*, *31*, 431–440.

Levin, I., H. Glatzel-Mattheier, T. Marik, M. Cuntz, M. Schmidt, and D. E. Worthy (1999), Verification of German methane emission inventories and their recent changes based on atmospheric observations, *J. Geophys. Res.*, *104*, 3447–3456.

Levin, I., B. Kromer, M. Schmidt, and H. Sartorius (2003), A novel approach for independent budgeting of fossil fuels CO_2 over Europe by $^{14}CO_2$ observations, *Geophys. Res. Lett.*, *30*(23), 2194, doi:10.1029/2003GL018477.

Majewski, D. (1991), The Europamodell of the Deutscher Wetterdienst, in *Numerical Methods in Atmospheric Models*, vol. 2, pp. 147–191, Eur. Cent. for Medium-Range Weather Forecasts, Reading, UK.

Müller, J.-F. (1992), Geographical distribution and seasonal variation of surface emissions and deposition velocities of atmospheric trace gases, *J. Geophys. Res.*, *97*, 3787–3804.

Neubert, R. E. M., L. L. Spijkervet, J. K. Schut, H. A. Been, and H. A. J. Meijer (2004), A computer-controlled continuous air drying and flask sampling system, *J. Atmos. Oceanic Technol.*, *21*, 651–659.

Olivier, J. G. J., J. A. Van Aardenne, F. Dentener, L. Ganzeveld, and J. A. H. W. Peters (2005), Recent trends in global greenhouse gas emissions: Regional trends and spatial distribution of key sources, in *Non-CO_2 Greenhouse Gases (NCGG-4)*, pp. 325–330, Millpress, Rotterdam.

Potosnak, M. J., S. C. Wofsy, A. S. Denning, T. J. Conway, J. W. Munger, and D. H. Barnes (1999), Influence of biotic exchange and combustion sources on atmospheric CO_2 concentrations in New England from observations at a forest flux tower, *J. Geophys. Res.*, *104*, 9561–9569.

Prather, M., D. Ehalt, F. Dentener, R. Derwent, E. Dlugokencky, E. Holland, I. Isaksen, J. Katima, V. Kirchhoff, and P. Matson (2001), Atmospheric chemistry and greenhouse gases, in *Climate Change 2001: The Scientific Basis, Contribution of Working Group I to the Third Assessment Report of the Intergovernmental Panel on Climate Change*, edited by J. T. Houghton et al., chap. 4, pp. 239–287, Cambridge Univ. Press, New York.

Rivier, L., P. Ciais, D. A. Hauglustaine, P. Bakwin, P. Bousquet, P. Peylin, and A. Klonecki (2006), Evaluation of SF_6, C_2Cl_4, and CO to approximate fossil fuel CO_2 in the Northern Hemisphere using a chemistry transport model, *J. Geophys. Res.*, *111*, D16311, doi:10.1029/2005JD006725.

Roeckner, E., K. Arpe, L. Bengtsson, M. Christoph, M. Claussen, L. Duemenil, M. Esch, M. Giorgetta, U. Schlese, and U. Schulzweida (1996), The atmospheric general circulation model ECHAM-4: Model description and simulation of present-day climate, *Rep. 218*, 90 pp., Max Planck Inst. for Meteorol., Hamburg, Germany.

Sanhueza, E., Y. Dong, D. Scharffe, J. M. Lobert, and P. J. Crutzen (1998), Carbon monoxide uptake by temperate forest soils: The effects of leaves and humus layers, *Tellus, Ser. B*, *50*, 51–58.

Schmidt, M., H. Glatzel-Mattheier, H. Sartorius, D. E. Worthy, and I. Levin (2001), Western European N_2O emissions: A top-down approach based on atmospheric observations, *J. Geophys. Res.*, *106*, 5507–5516.

Shindell, D. T., J. L. Grenfell, D. Rind, V. Grewe, and C. Price (2001), Chemistry-climate interactions in the Goddard Institute for Space Studies general circulation model: 1. Tropospheric chemistry model description and evaluation, *J. Geophys. Res.*, *106*, 8047–8075.

Spivakovsky, C. M., et al. (2000), Three-dimensional climatological distribution of tropospheric OH: Update and evaluation, *J. Geophys. Res.*, *105*, 8931–8980.

Stuiver, M., and H. A. Polach (1977), Discussion: Reporting of ^{14}C data, *Radiocarbon*, *19*, 355–363.

Stuiver, M., and P. Quay (1981), Atmospheric ^{14}C changes resulting from fossil fuel CO_2 release and cosmic ray flux variability, *Earth Planet. Sci. Lett.*, *53*, 349–362.

Suess, H. E. (1955), Radiocarbon concentration in modern wood, *Science*, *122*, 415–417.

Takahashi, T., R. H. Wanninkhof, R. A. Feely, R. F. Weiss, D. W. Chipman, N. Bates, J. Olafsson, C. Sabine, and S. C. Sutherland (1999), Net sea-air CO_2 flux over the global oceans: An improved estimate based on the sea-air pCO_2 difference, paper presented at 2nd CO_2 in Oceans Symposium, Cent. for Global Environ. Res., Natl. Inst. for Environ. Stud., Tsukuba, Japan, 18–23 Jan.

Tans, P. P., A. F. M. de Jong, and W. G. Mook (1979), Natural atmospheric ^{14}C variation and the Suess effect, *Nature*, *280*, 826–827.

Turnbull, J. C., J. B. Miller, S. J. Lehman, P. P. Tans, R. J. Sparks, and J. Southon (2006), Comparison of $^{14}CO_2$, CO, and SF_6 as tracers for recently added fossil fuel CO_2 in the atmosphere and implications for biological CO_2 exchange, *Geophys. Res. Lett.*, *33*, L01817, doi:10.1029/2005GL024213.

van der Plicht, J., S. Wijma, A. T. Aerts, M. H. Pertuisot, and H. A. J. Meijer (2000), The Groningen AMS facility: Status report, *Nucl. Instrum. Methods Phys. Res., Sect. B*, *172*, 58–65.

Wickert, B. (2001), Berechnung anthropogener Emissionen in Deutschland für Ozonsimulationen: Modellentwicklung und Sensitivitätsstudien, dissertation, Inst. für Energiewirt. und Rationelle Energieanwendung, Univ. Stuttgart, Stuttgart, Germany.

Worthy, D., and L. Huang (Eds.) (2005), Proceedings of the 12th WMO/IAEA Meeting of Experts on Carbon Dioxide Concentrations and Related Tracers Measurement Techniques, Toronto, Canada, 15–18 September 2003, *WMO-Rep. 161, TD 1275*, World Meteorol. Organ. Global Atmos. Watch, Geneva.

Zondervan, A., and H. A. J. Meijer (1996), Isotopic characterization of CO_2 sources during regional pollution events using isotopic and radiocarbon analysis, *Tellus, Ser. B*, *48*, 601–612.

U. Gamnitzer, Lehrstuhl für Grünlandlehre, Technische Universität München, Am Hochanger 1, D-85350 Freising-Weihenstephan, Germany.

U. Karstens, Max Planck Institute for Biogeochemistry, Hans-Knöll-Straße 10, D-07745 Jena, Germany.

B. Kromer, Heidelberger Akademie der Wissenschaften, INF 229, D-69120 Heidelberg, Germany.

I. Levin and H. Schroeder, Institut für Umweltphysik, University of Heidelberg, Building INF 229, D-69120 Heidelberg, Germany. (ingeborg.levin@iup.uni-heidelberg.de)

H. A. J. Meijer and R. E. M. Neubert, Centrum voor IsotopenOnderzoek, University of Groningen, Nijenborgh 4, NL-9714 AG Groningen, Netherlands.